Scheidt *et al. Swiss Journal of Geosciences* (2023) 116:12
https://doi.org/10.1186/s00015-023-00439-y

SGG SGS sc | nat
Swiss Journal of Geosciences

ORIGINAL PAPER Open Access

Palaeomagnetic and mineral magnetic analyses of the Deckenschotter of northern Switzerland and southern Germany

Stephanie Scheidt[1*], Marius W. Buechi[2], Ramon Egli[3], Andrea R. Biedermann[4] and Gaudenz Deplazes[5]

Abstract

The Deckenschotter is a fluvial to glaciofluvial gravel unit in northern Switzerland and southern Germany. The deposits are considered the oldest preserved glacial to interglacial Quaternary deposits in the northern Alpine foreland and are thus important geomorphological markers for landscape evolution. Nevertheless, the age of the deposits is only approximately known and subject to controversial debates. This study presents the results of an extensive palaeomagnetic investigation carried out on intercalated fine-grained sediments at 11 sites of the Höhere Deckenschotter (HDS) and at 5 sites of the Tiefere Deckenschotter (TDS). The HDS show reversed and normal magnetisations, indicating deposition > 0.773 Ma, while the TDS exhibit only normal directions. Age constraints for the different sites are discussed in the light of evidence from other studies. The study therefore clearly supports the efforts to determine the age of the Deckenschotter. As data from previous palaeomagnetic studies on the HDS and TDS have not been published or preserved, this is in fact the only data-based palaeomagnetic study available.

Keywords Magnetic polarity stratigraphy, Tiefere Deckenschotter, Höhere Deckenschotter, Sediment, Switzerland, Germany, Quaternary, Alpine foreland, Glacial, Interglacial

1 Introduction

The morphostratigraphically derived classification of deposits of the northern central Alpine foreland distinguishes four units (Fig. 1; Graf and Burkhalter, 2016): the 'Höherer Deckenschotter' (HDS), 'Tieferer Deckenschotter' (TDS), 'Hochterrasse' (HT) and 'Niederterasse' (NT). These deposits represent different stages of the landscape reorganisation during the Quaternary period that was basically controlled by uplift and erosion (e.g., Schlunegger and Hinderer, 2001), and the intensification of Alpine glaciation (e.g., Haeuselmann et al., 2007; Preusser et al., 2011; Valla et al., 2011). The Deckenschotter deposits are thought to be the oldest preserved glacial to interglacial Quaternary deposits in the northern Alpine foreland (Preusser et al., 2011), and therefore of high scientific importance as geomorphological markers for the formerly existing fluvial channel network.

The German name Deckenschotter (literally cover gravels) is a relic from a time when the deposits were thought to represent the remains of glacial advances deposited on large plains. Since the beginning of the twentieth century the older, upper HDS and the younger, lower, TDS are interpreted as infills of wide fluvial channels in the

Handling editor: György Hetényi

*Correspondence:
Stephanie Scheidt
stephanie.scheidt@uni-koeln.de
[1] Institute of Geology and Mineralogy, University of Cologne, Zülpicher Str. 49a, 50674 Cologne, Germany
[2] Institute of Geological Sciences and Oeschger Centre for Climate Change Research, University of Bern, Baltzerstrasse 1+3, 3012 Bern, Switzerland
[3] Department of Geophysics, GeoSphere Austria, Hohe Warte 38, 1190 Vienna, Austria
[4] Institute of Geological Sciences, University of Bern, Baltzerstrasse 1+3, 3012 Bern, Switzerland
[5] National Cooperative for the Disposal of Radioactive Waste (Nagra), Hardstrasse 73, 5430 Wettingen, Switzerland

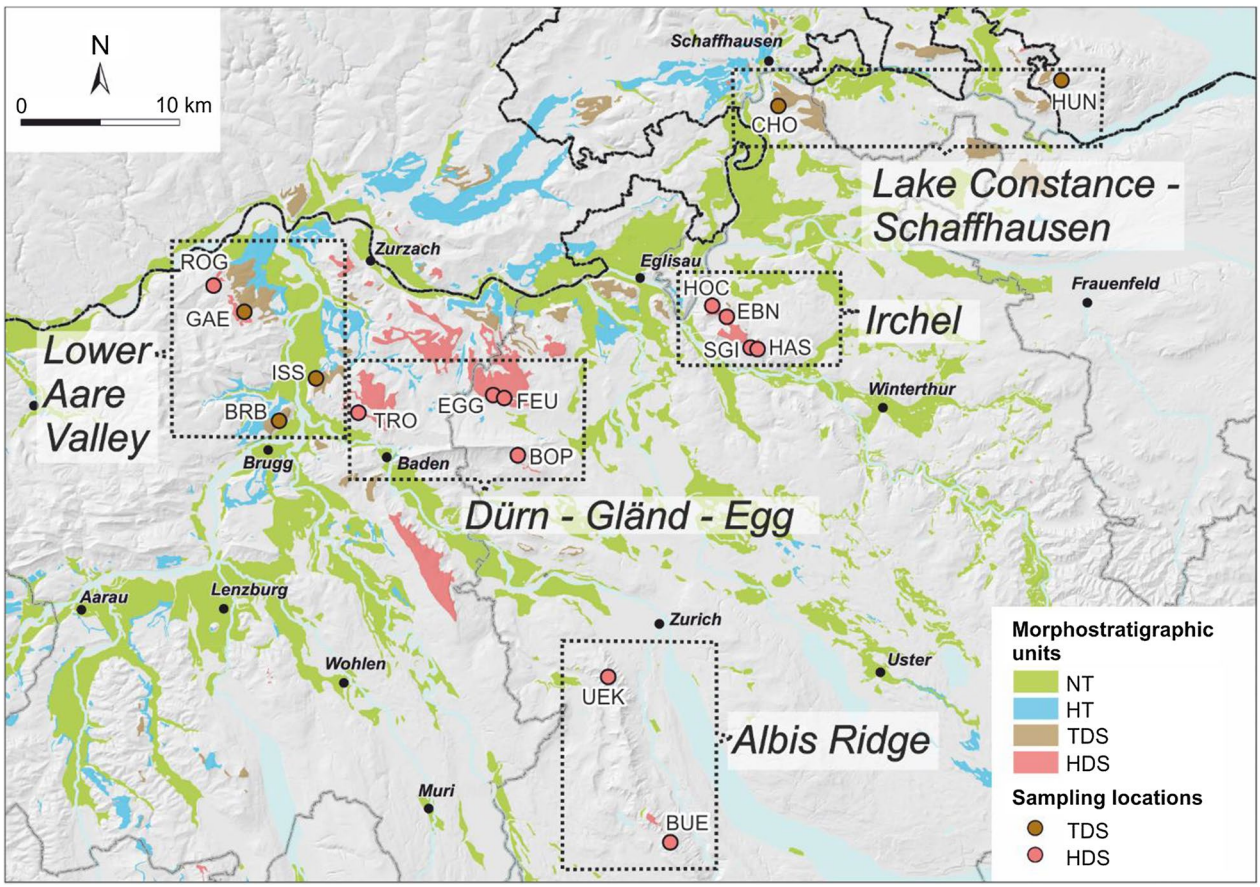

Fig. 1 Map of the sampling locations with assignment to the regions used in this study as well as the distribution of the Höherer Deckenschotter (HDS), Tieferer Deckenschotter (TDS), Hochterrasse (HT), and Niederterrasse (NT) in northern Switzerland and southern Germany. HDS sites: *BOP* Boppelsen Cholholz, *BUE* Bürglen, *EBN* Irchel Ebni, *EGG* Egghalden Schleinikon, *FEU* Feusi Oberweningen, *HAS* Irchel Hasli, *HOC* Irchel Hochwacht, *ROG* Roggenfeld Mettauertal, *SGI* Irchel Steig, *TRO* Tromsberg, *UEK* Uetliberg Kulm. TDS sites: *BRB* Bruggerberg, *CHO* Cholfirst/ Kiesgrube Chirchhölzli Laufen-Uhwiesen, *GAE* Ängi Mandach, *ISS* Iberig Würenlingen, *HUN* Hungerbol

moderate-relief palaeolandscape of the Alpine foreland (Frei, 1912; Graf, 1993; Hantke, 1962; Penck & Brückner, 1909; Preusser et al., 2011, and references therein). They consist mainly of fluvial to glaciofluvial gravels, which are occasionally intercalated by glaciogenic diamicts, overbank deposits and palaeosols. The HDS and TDS are separated by a period of considerable incision, but each unit has a multiphase sedimentation history, suggesting aggradation in proglacial areas during the glacials and markedly altered sedimentation patterns during interglacials (Graf, 1993, 1996, 2009).

Due to the high importance of the Deckenschotter for the reconstruction of landscape evolution, various attempts have been made to determine the age of these deposits. Initially, a number of authors discussed the glacial assignment of the Deckenschotter to the glacials Würm, Riss, Mindel and Günz solely on the basis of geomorphological and lithostratigraphic features (e.g., Frei, 1912; Güller, 1944; Hantke, 1962; Weber, 1930, and reference therein). First palaeomagnetic measurements were conducted in southern Germany in the 1980s (Rolf et al., 2012). However, the results only have a regional significance, because the classification systems of the Deckenschotter in Bavaria, Baden-Württemberg, Austria and Switzerland are different and the stratigraphic position of the different units has not been conclusively clarified (Doppler et al., 2011). Graf (1993) used a multi-proxy approach that include palynological and molluscan evidence in addition to traditional methods. Furthermore, he performed the first palaeomagnetic investigations on the Deckenschotter and suggested that the HDS was deposited either during the Jaramillo subchron (1.07–0.99 Ma) or an earlier time that allows acquisition of a normal-polarity characteristic remanent magnetisation (ChRM) prior to the Brunhes Chron. Bolliger et al. (1996) identified key marker species in the HAS site of the HDS that belong to the mammal fauna

biozone MN 17 (2.6–1.8 Ma; Fejfar & Heinrich, 1990). They supplemented their study with palaeomagnetic investigations and, thereby, reinforced the results of Graf (1993). Recently, studies using cosmogenic nuclide dating provide age constraints on the timing of emplacement of the HDS and TDS. Accordingly, the HDS deposits have an age between 2.5 Ma and 1 Ma (Akçar et al., 2014, 2017; Claude et al., 2019; Dieleman et al., 2022). However, Knudsen et al. (2020) applied an additional modelling step to account for variable cosmic-ray exposure and non-steady erosion and propose an age of around 1.0–0.9 Ma for the accumulation of the HDS and in turn for the onset of major glaciation in the Alps. Particularly controversial is the ~ 0.9 Ma age for HDS deposits from Irchel Plateau in Switzerland. Based on this proposed age, Claude et al. (2019) call for a revision of the lithostratigraphy of Deckenschotter sediments, and Dieleman et al. (2022) propose a formation of the Deckenschotter deposits in even more complex cut-and-fill cycles. Furthermore, they argue that a morphostratigraphic subdivision of the Deckenschotter deposits into HDS and TDS may not be consistent with the chronostratigraphy. Overall, and despite all efforts, the age of the HDS and the TDS, as well as the age of the separating incision period, remains poorly constrained.

To assist future studies with a comprehensive palaeomagnetic data set, this study presents an extended palaeomagnetic survey, including 16 sites of the HDS and TDS (Fig. 1). The palaeomagnetic work is complemented with analyses of the magnetic mineralogy and the magnetic fabric to provide evidence for the reliability and origin of the carriers of the magnetisation. The sites EBN, HOC, EGG, ROG and HAS in the studies by Graf (1993) and Bolliger et al. (1996), were re-examined, as their measurement data are not preserved in data repositories. This also applies to the palaeomagnetic investigations of the BUE and UEK sites recently published by Graf (2019). Thus, this work represents the first comprehensive, data-backed study of the magnetic behaviour of the Deckenschotter deposits.

2 Working area and methodology

2.1 Working area, field work and sample preparation

Extensive site investigations were carried out by Nagra with the aim of finding occurrences of finer sediments in the Deckenschotter for various analyses. These are sediments deposited in floodplains or accumulated in

Table 1 Basic information about the sites and the number of samples taken different depths level within each site

Site name	Site abbreviation	Unit	Region (in this study)	Depth level sampled	Samples analysed	CH1903 coordinates	
						X	Y
Irchel Hochwacht	HOC	HDS	Irchel Plateau	9	23	686,075	268,269
Irchel Ebni	EBN	HDS	Irchel Plateau	6	13	687,007	267,577
Irchel Steig	SGI	HDS	Irchel Plateau	7	8	688,500	265,633
Irchel Hasli	HAS	HDS	Irchel Plateau	28	30	688,943	265,570
Uetliberg Kulm	UEK	HDS	Albis Ridge	15	31	679,605	244,805
Bürglen	BUE	HDS	Albis Ridge	6	11	683,435	234,430
Kiesgrube Tromsberg Kirchdorf	TRO	HDS	Dürn–Gländ–Egg	1	0	663,770	261,525
Egghalden Schleinikon	EGG	HDS	Dürn–Gländ–Egg	8	11	672,230	262,630
Boppelsen Cholholz	BOP	HDS	Dürn–Gländ–Egg	8	10	673,664 673,656	258,893 258,899
Feusi Oberwenigen	FEU	HDS	Dürn–Gländ–Egg	7	7	672,950	262,450
Roggenfeld Mettauertal	ROG	HDS[a]	Lower Aare Valley	17	22	654,680	269,605
Ängi Mandach	GAE	TDS	Lower Aare Valley	2	2	656,610	267,925
Iberig Würenlingen	ISS	TDS	Lower Aare Valley	13	14	661,070	263,700
Bruggerberg Brugg	BRB	TDS	Lower Aare Valley	3	3	659,040 to 658,995	261,075 to 261,045
Cholfirst/Kiesgrube Chirchhölzli Laufen-Uhwiesen	CHO	TDS	Lake Constance–Schaffhausen	3	4	690,250	280,875
Hungerbol Öhningen	HUN	TDS	Lake Constance–Schaffhausen	29	47	708,100	282,505

The table is arranged according to the regions shown in Fig. 1 and in the order in which they are presented in this study

[a] The in geological maps established assignment of ROG to HDS is challenged in this study (see Sect. 4)

low-energy zones of the fluvial depositional environment. With the exception of the HUN site in Germany, all of the investigated sites are located in northern Switzerland (Fig. 1). Basic information on the sites is provided in Table 1. Additional site descriptions and information on further literature to individual sites are given in the supplementary material. In order to present the sites concisely this study distinguishes between five different regions (Fig. 1). All regions, other than the Lower Aare Valley, contain either HDS or TDS.

Sampling took place in a pilot study in September 2016, and two following field campaigns in July 2017 and August 2018. Due to the difficult sampling situation, only a limited number of samples could be taken at certain sites. This was the case at sites FEU, CHO, and most of ISS, where individual outcrops were only accessible by rope descent. Due to the loose nature of the gravel, the outcrop had been cleared of loose debris by climbing specialists beforehand.

Surfaces exposed to weathering were removed before sampling. When possible, oriented samples were taken by pushing one-inch wide cylindrical tubes into the soft sediment surface. In cases where the sediment was too hard for this technique, oriented sediment blocks were prepared from the outcrops and plastered for transportation. The orientation of the cylindrical tubes and the hand pieces was measured with a magnetic compass. Samples were dried in the laboratory and, if necessary, treated with stone hardener (oH G30, Schmalstieg GmbH, Germany) to prevent collapse. Cylindrical samples yielded up to three subsamples. The plastered handpieces were sawn into a certain number of subsamples according to their size. Orientation marks were carefully copied to each subsample. See the supplementary material for information on the naming scheme applied. No subsamples could be produced from the single, medium to fine sand sample from TRO, as it collapsed due to a lack of binding agents.

2.2 Palaeomagnetic and mineral magnetic analyses

Palaeomagnetic and magnetic mineral measurements were conducted at the Leibniz Institute for Applied Geophysics (Hannover, Germany), the Eberhard Karls University (Tübingen, Germany), the Swiss Federal Institute of Technology (ETH, Zürich, Switzerland), and the University of Cologne (Cologne, Germany) using different devices and measurement protocols (see Additional file 1: Table S1 for details). The natural remanent magnetisation (NRM) of all samples was measured with 2G Enterprise (Mountain View, CA, USA) cryogenic magnetometers. Subsequently, the low-field magnetic susceptibility (χ) was determined using AGICO (Brno, CZ) Kappabridges. Following the protocols of individual laboratories, alternating field (AF) demagnetisation was conducted in up to 20 progressively increasing demagnetisation steps up to a maximum of 120, 150, or 300 mT and thermal (TH) demagnetisation experiments were conducted in up to 17 heating steps up to 600–700 °C. Minor differences resulting from the use of different equipment for the same kind of analyses are irrelevant for our applications, which aims only on magnetic polarity stratigraphy.

The ChRM was isolated by principal component analysis (PCA) using the software Remasoft 3.0 by AGICO (Chadima and Hrouda, 2006). The ChRM was determined by including the origin of the Zijderveld diagram in the linear segments; anchoring was only applied when grouping of the data points would otherwise have prevented the ChRM from being determined. The number of steps used to determine the ChRM is presented in Additional file 1: Table S2. Mean directions were calculated by Remasoft 3.0 using Fisher statistics (Fisher, 1953). The frequency dependency of magnetic susceptibility (χ_{FD}) was determined by measuring χ at two frequencies (χlf at 505 Hz and χ_{hf} at 5050 Hz) using a Magnon VFSM susceptibility bridge. χ_{FD} is defined as:

$$\chi_{FD}(\%) = 100\,[(\chi_{lf} - \chi_{hf})/\chi_{lf}]. \quad (1)$$

Isothermal remanent magnetisation (IRM), backfield curves, and hysteresis loops were measured in fields up to 1.5 T using a Lake Shore vibrating sample magnetometer (VSM) model 8604. The saturation magnetisation M_s was determined with the approach to saturation method of Fabian (2006) by fitting the closed range of hysteresis loops with

$$M(B) = M_s + \chi_{hf}B + \alpha B^{\beta}, \quad (2)$$

where B is the applied field, and M_s, χ_{hf}, and β model parameters that minimise the squared model residuals. The saturation remanence M_{rs}, coercive field B_c, and coercivity of remanence B_{cr} were determined using local polynomial fits of the measured hysteresis and backfield curve around $B=0$ and $M=0$. In some cases (e.g., samples EGG2-02, HUN2-01B) the hysteresis loop is heavily undersaturated at the maximum field of 1.5 T, due to the presence of high-coercivity minerals, leading to an underestimation of M_s, and consequently to overestimated M_{rs}/M_s in the Day diagram. This is not a problem, as long as the Day diagram is used to detect relative differences between the hysteresis loops.

2.3 Magnetic fabrics

The magnetic fabrics of nine selected subsamples from UEK and one subsample from EGG were characterized in the Laboratory of Natural Magnetism, ETH Zurich, Switzerland. Samples from UEK were selected because of its

quite flat ChRM inclination values. The single EGG subsample was added for comparison.

Several types of magnetic fabric measurements were used to determine and compare the anisotropy associated with various grain populations in the rocks: anisotropy of magnetic susceptibility (AMS), anisotropy of anhysteretic remanent magnetisation (AARM), and anisotropy of full and partial isothermal remanent magnetisation (AIRM, ApIRM). While AMS is a superposition of the anisotropies from all grains, para-, dia- and ferromagnetic, remanence anisotropy targets only the remanence-carrying portion of the ferromagnetic grains. To divide this latter group further, AARM was used to capture low-coercivity remanence carriers, and ApIRMs for the high-coercivity remanence carriers. AMS was measured on an AGICO MFK1-FA susceptibility bridge, in a field of 200 A/m and frequency of 976 Hz. Depending on the sample size, the susceptibility tensor was either determined from 15 directional measurements (Jelínek, 1977), or from differential measurements in three mutually perpendicular planes (Jelinek, 1996). AARM and A(p)IRM were determined using nine directional measurements, and computing the tensors from the magnetisation components parallel to the applied field (McCabe et al., 1985). Directional ARMs were imparted on an inline AF/ARM system of the 2G superconducting rock magnetometer (SRM), with a DC bias field of 0.1 mT applied over an AF window of 0–140 mT. After the magnetisation was measured on the 2G SRM, samples were demagnetised at 150 mT AF. Any ARM that could not be demagnetized at 150 mT AF was subtracted as background. IRMs were imparted on an ASC Scientific IM-10-30 pulse magnetiser, in a field of 1 T, followed by a field of 100 mT. The latter was applied to avoid any artefacts due to the backfield of the former. IRMs were measured on the 2G SRM. To measure pIRMs, the IRMs imparted on the pulse magnetiser were AF demagnetised on the 2G inline AF system to 100 mT and 140 mT prior to measurement of the magnetisation.

Susceptibility and ARM susceptibility are symmetric second-order tensors, and can be characterised by their mean susceptibility k_{mean}, and the eigenvalues $k_1 \geq k_2 \geq k_3$ and associated eigenvectors. Anisotropy is described here by the corrected degree of anisotropy P' and the shape parameter T (Hrouda, 1982; Jelinek, 1981):

$$P' = \left(\frac{k_1}{k_3}\right)^a, a = \sqrt{1 + \frac{T^2}{3}} \quad (3)$$

$$T = (2 * \ln(k_2) - \ln(k_1) - \ln(k_3))/(\ln(k_1) - \ln(k_3)) \quad (4)$$

The shape of the AMS ellipsoid is oblate if $0 < T < +1$ (the magnetic fabric is planar) and rotational oblate if $T = +1$. The shape of the AMS is prolate if $-1 < T < 0$ (the magnetic fabric is linear) and rotational prolate if $T = -1$.

Being a non-linear function of applied field, describing AIRM and ApIRM by tensor mathematics is strictly not correct (Coe, 1966), but it is often a good approximation (Biedermann et al., 2019). Therefore, AIRM and ApIRM will be described here by the same tensor mathematics as AMS and AARM.

3 Results and interpretation

Most of the fine-grained intercalations sampled in the TDS and HDS do not have ideal physical properties for palaeomagnetic analyses. Sediments are often relatively coarse, contain insect burrows and are affected by diagenetic overprinting. Therefore, it is likely that samples contain large magnetic grains with poor ChRM conservation potential, show orientation disturbances, and carry only viscous and secondary magnetisations instead of the desired post detrital remanent magnetisation (pDRM) or detrital remanent magnetisation (DRM). Indeed, a large number of samples were considered unreliable and discarded. Only 21 of 70 TDS subsamples and 69 of 166 HDS subsamples provided results that were considered in this study; all subsamples were excluded from three of the 16 sites. The data of samples with unstable demagnetisation paths, low temperature stability (i.e., largely demagnetised below ~ 350 °C), low coercivity (largely demagnetisation below ~ 40 mT) and inconsistent ChRM directions (i.e., inclinations and declinations with conflicting polarity) were rejected (Additional file 1: Fig. S1). Thereby, all coarser grained subsamples (i.e., dominated by fine to medium sand) were discarded. Since there have been no significant changes in the position of the study area with respect to the magnetic poles since the Pliocene (Besse and Courtillot, 2002), the samples whose ChRM direction deviated significantly from the present-day Earth's magnetic field (EMF) or its reverse counterpart were also discarded (Additional file 1: Fig. S1). These samples have been likely affected by currents during deposition or diagenetic processes, which can significantly disturb the alignment of magnetic grains (Griffiths et al., 1960; Tanty et al., 2016). The present geomagnetic field in the working area show negligible variability (Fischer & Schnegg, 1979a, 1979b) with declination and inclination around 2° and 63°, respectively [international geomagnetic reference field model (NOAA, 2022)].

Table 2 NRM and magnetic susceptibility ranges of the samples finally also used for magnetic polarity stratigraphy

	Minimum	Maximum	Mean	Median
HDS NRM	2.21×10^{-8} Am^2 kg^{-1}	1.56×10^{-5} Am^2 kg^{-1}	3.40×10^{-6} Am^2 kg^{-1}	1.69×10^{-6} Am^2 kg^{-1}
HDS magnetic susceptibility	2.85×10^{-8} m^3 kg^{-1}	9.65×10^{-8} m^3 kg^{-1}	5.53×10^{-8} m^3 kg^{-1}	5.37×10^{-8} m^3 kg^{-1}
TDS NRM	2.38×10^{-8} Am^2 kg^{-1}	4.57×10^{-6} Am^2 kg^{-1}	6.73×10^{-7}Am^2 kg^{-1}	1.15×10^{-7} Am^2 kg^{-1}
TDS magnetic susceptibility	1.01×10^{-8} m^3 kg^{-1}	9.11×10^{-8} m^3 kg^{-1}	4.09×10^{-8} m^3 kg^{-1}	3.90×10^{-8} m^3 kg^{-1}

3.1 Magnetic mineralogy

The mineral magnetic investigations aim at verifying the primary origin of the NRM as DRM or pDRM, and eventually the reliability of the polarity stratigraphy. An exact determination or quantification of the individual magnetic mineral components of the HDS and TDS deposits is, however, beyond the scope of this study.

Although χ of the HDS and TDS display comparable readings (Table 2), the range of values of the NRM of the TDS is broader and the maximum, median, and mean values are an order of magnitude weaker than those of

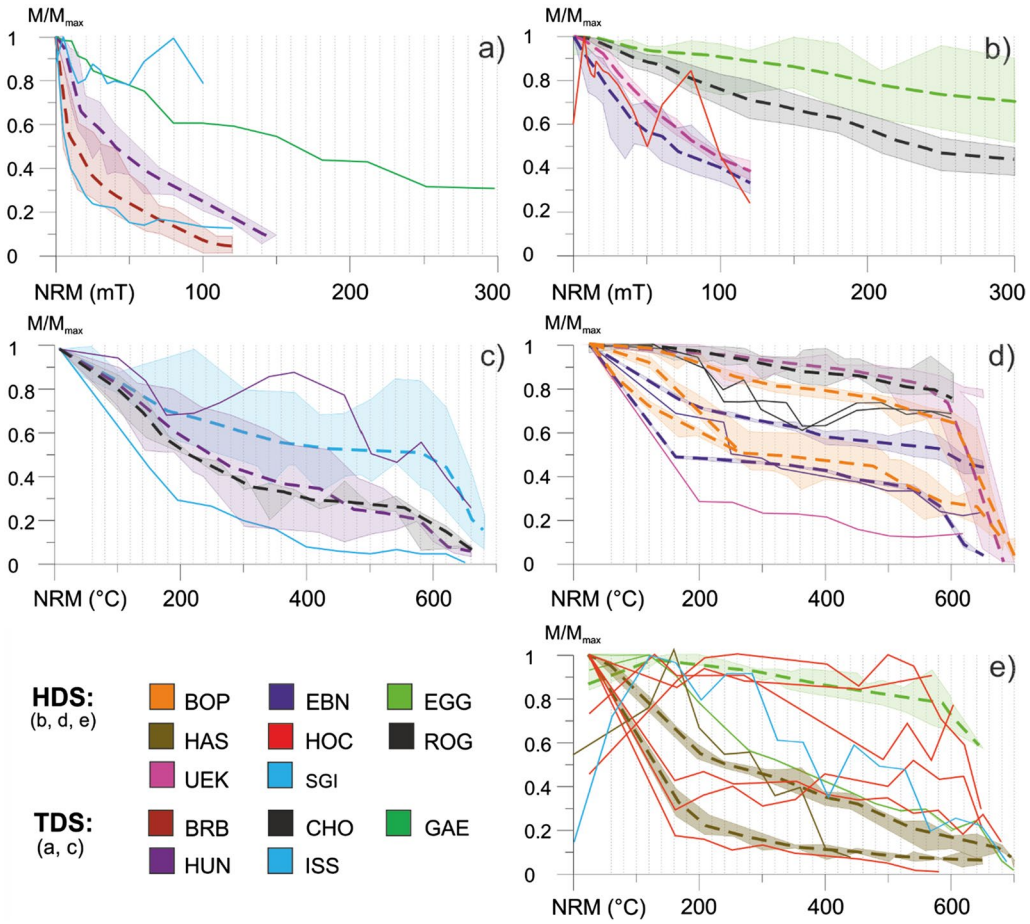

Fig. 2 Normalised magnetisation vs. demagnetisation steps of the final sample set. The range of demagnetisation curves is shown in colour-coded transparent areas. Typical features of the demagnetisation behaviour are illustrated as inferred trendlines (dashed lines). Demagnetisation curves diverging from the indicated trends of the respective sites are shown individually. **a** AF demagnetisation of TDS samples from CHO (n = 2), HUN (n = 5), ISS (n = 6). **b** AF demagnetisation of HDS samples from, EBN (n = 3), EGG (n = 4), HOC (n = 1), ROG (n = 3), UEK (n = 4). **c** TH demagnetisation of TDS samples from BRB (n = 3), GAE (n = 1), HUN (n = 2), ISS (n = 2). **d** TH demagnetisation of HDS samples from BOP (n = 8), EBN (n = 5), ROG (n = 10), UEK (n = 13). **e** TH demagnetisation of HDS samples from EGG (n = 4), HAS (n = 7), HOC (n = 6), SGI (n = 1); Please note that no trend is given for samples from HOC. All individual demagnetisation paths are available in (Scheidt et al., 2023)

the HDS. The sediment profiles of the HDS sites EBN, HOC, and HAS, as well as the TDS site HUN are characterised by a downward decreasing trend of NRM and χ (see "Samples-Results" in Scheidt et al., 2023), which likely reflects a corresponding trend in the concentration of remanence carriers. The presence of iron and manganese redox fronts (e.g., Additional file 1: Figs. S5, S17) suggest that the decrease in magnetic mineral concentration is related to iron leaching processes, which are probably associated with groundwater fluctuations (Rezanezhad et al., 2014). Evidence of iron mineral dissolution is also found at other sites and may explain the variability of NRM and χ-values.

Constraints on the mineral magnetic composition carrying the remanent magnetisation is gained from NRM demagnetisation experiments (Fig. 2). The AF demagnetisation paths of the HDS and TDS start with a more or less pronounced drop over the 0–20 mT range, followed by a more gradual decrease at larger fields. With the exception of the TDS sites BRB and HUN, and some samples from the HDS site HAS, all samples maintain > 19% residual magnetisation. Consequently, the NRM of the TDS and HDS deposits, is carried by variable portions of a low coercivity component (AF demagnetisation at < 20 mT), an intermediate component (AF demagnetisation at 20–100 mT), and a high coercivity component (not AF demagnetised up to 100 mT).

The NRM fraction that is AF demagnetised at 20 mT likely consists essentially of viscous remanent magnetisations (VRMs) and very soft magnetisations, unsuitable for magnetic polarity stratigraphy. Since the samples of the FEU site were full demagnetised in low fields and showed typical directional instability (Additional file 1: Fig. S11), all samples of the site were discarded.

The intermediate component is probably largely carried by common detrital ferrimagnetic minerals, such as pure or cation-substituted magnetite, maghemite, and members of the titanomagnetite and ilmenohaematite solid solution series (Johnson et al., 1975, Heider et al., 1992, Brown and McEnroe, 2004). These minerals cannot be easily differentiated either by their coercivity or by their Curie temperature (T_C). However, the gradual NRM decrease in the TH demagnetisation experiments above 200 °C is compatible with these minerals (Nishitani and Kono, 1983, Harrison and Putnis, 1996, Gehring et al., 2009, Jiang et al., 2016). Furthermore, few samples of the TDS sites CHO and HUN, and the HDS site EBN exhibit inflections of the thermal demagnetisation curves around the T_C of pure magnetite at 580 °C (Fig. 2). Although the minerals suggested for the intermediate coercivity component are important DRM and pDRM carriers, they may also carry a chemical remanent magnetisation (CRM), if surface oxidation after deposition reduces the domain state of ferrimagnetic particles from multi-domain (MD) to vortex (Heider and Dunlop, 1987; Cui et al., 1994). However, averaged over the large number of magnetic particles within a bulk palaeomagnetic sample, it is likely that the DRM direction will be retained, as not all grains will re-orientate their magnetisation (Almeida et al., 2014). In suitable environmental and climatic conditions magnetite in single-domain (SD) or vortex state may also form authigenically in silts, sands, and soils (Maher, 1986, Taylor et al., 1986, Maher and Taylor, 1988). Such fine-grained secondary minerals are usually characterised by elevated χ_{FD} values. Thus, the detrital origin of magnetite in the Deckenschotter samples is supported by low χ_{FD} values of 53 subsamples from 10 HDS and TDS sites (Additional file 1: Table S2) that reach only 1.64% (mean of 0.74%). Another secondary ferrimagnetic mineral that possibly contribute to the intermediate coercivity group forms from dissolved iron in water-saturated sediments (Fassbinder and Stanjek, 1994, Rowan and Roberts, 2006): greigite can be identified by its strong tendency to acquire a gyroremanent magnetisation (GRM) during AF treatment (Snowball, 1997, Stephenson and Snowball, 2001). An increase in magnetisation between 200 °C and 400 °C may also be attributed to the irreversible alteration of this or other secondary minerals. Due to exclusion of all samples showing GRM or alteration features, all samples from BUE were discarded (Additional file 1: Fig. S6). However, in a few cases in which the directional orientation remained stable during TH demagnetisation up to temperature > 500 °C and/or the stable isolated ChRM direction corresponded to neighbouring samples, subsamples remained in the sample set even though there were indications for alteration of secondary minerals. This applies in particular to the samples of HOC and HUN. Finally, depending on the domain state, the particle shape and internal stress of particles, haematite may also get partially demagnetised in AF fields up to 100 mT (Dankers, 1981) and contribute thus, to the intermediate coercivity component of the sediments.

The contributions with high coercivity in HDS and TDS are probably mainly due to goethite, haematite and martite, but possibly also to surface oxidised (titanium) magnetite and maghemite particles (e.g., Johnson and Merrill, 1973, France and Oldfield, 2000, Maher et al., 2003, Almeida et al., 2014, Ge and Williams, 2020). All of these minerals are potentially able to reliably record the EMF. For detrital minerals, this signal is usually a DRM or pDRM carried by particles in single-domain (SD) and vortex state. However, the high coercivity fraction may also carry a CRM, if goethite and hematite form authigenically (e.g., Gendler et al., 2005; Jiang et al., 2015, 2018). In general, goethite is preferentially formed in cool, moist soils that rarely have prolonged dry periods,

while haematite is more common in subtropical, Mediterranean or tropical soils with frequent episodes of prolonged drought (Schwertmann, 1988). From this point of view, the formation of haematite in the glaciofluvial environment of the Deckenschotter is less likely than that of goethite. Assuming that sister samples are composed identical, the relative contributions of goethite and hematite to the NRM can be estimated from the Neel temperatures (T_N) of 120 °C (Özdemir and Dunlop, 1996) and 600–690 °C (Jiang et al., 2015; Özdemir & Dunlop, 2005), respectively, if the residual NRM of an AF demagnetised sister samples is known. For example, from the drop in NRM of sample ISS1-01C by more than 50% after the 150 °C step (single line in Fig. 2c), only ~ 13% can be attributed to a high coercivity component, because the AF demagnetised sister sample ISS1-01B (lower single line in Fig. 2a; Additional file 1: Fig. S14) lost 87% of its NRM already with the 60 mT step. Since ~ 5% of the NRM of ISS1-01C was demagnetised only at > 600 °C and is thus likely due to haematite, only a maximum of ~ 8% of the NRM can be related to goethite. The remaining loss of NRM during the 150 °C TH demagnetisation step is probably due to VRMs and magnetic minerals with low blocking temperatures. In contrast, goethite appears to carry the dominant part of the magnetisation in a number of samples of the HAS site. Nevertheless, overall the contribution of goethite is rather small compared to haematite. In particular, this is indicated by the thermal demagnetisation curves of some HDS sites showing a plateau followed by a sharp drop between 600 °C and 690 °C. This drop is typical of a DRM carried by > 0.3 µm large haematite crystals (Swanson-Hysell et al., 2019; Jiang et al., 2022). Samples from the HDS sites EGG, ROG and UEK, but also some from HOC and CHO, are dominated by thermally highly stable magnetic mineral associations. By contrast, only few thermal demagnetisation curves of HAS (Fig. 2e) show a gradual trend up to full demagnetisation at 600–620 °C, as expected in the case of haematite-bearing CRM (Jiang et al., 2022). Combined with the absence of significant magnetic viscosity, the shape of the TH demagnetisation paths suggests a largely detrital origin of the haematite in the Deckenschotter sediments. The major significance of the minerals with high coercivity in all Deckenschotter deposits is also expressed by the fact that the acquisition curves of the IRM are usually not saturated at a field of 1.5 T and the hysteresis branches approach asymptotically to close only between 390 and 1500 mT (Fig. 3). As an expression of the varying composition and/ or domain states of the mineral magnetic associations, also the shapes of the hysteresis loops vary between potbellied and wasp-waisted (Roberts et al., 1995; Tauxe et al., 1996). Due to the multicomponent magnetic mineralogy, the samples also do not follow the mixing trends in the Day plot (Day et al., 1977; Dunlop, 2002) and the diagram cannot be used for domain state analyses (Roberts et al., 2019). Heavily undersaturated samples, such as some EGG and UEK ones, are characterised by unrealistically large values of M_{rs}/M_s and plot along or even above the SP saturation envelope, due to an underestimation of M_s. Samples with saturated hysteresis plot within the SD + MD and SP + SD mixing lines, reflecting mixed domain states typical of magnetic minerals with a wide grain size distribution.

3.2 Magnetic fabrics

The nine UEK and one EGG subsamples exhibit significant anisotropy, where the minimum susceptibility directions are well-defined, but the orientation of k_1 and k_2 in the k_1-k_2-plane is not always statistically significant, explaining the girdle distribution in the respective plane. The degree of remanence anisotropy (P' up to 1.56) is generally stronger than for AMS (P' < 1.08), and highest for ApIRM140-1000mT, except for sample UEK2-08 (same level as UEK2-07) whose AMS has the highest P'-value (P' = 1.74; Fig. 4) while its NRM and χ are not different compared to the neighbouring samples (Additional file 1: Table S2). The difference between this and the other samples examined was not investigated but may be due to the occurrence of shape anisotropic components such as, needle-shaped magnetite minerals or iron oxides.

Anisotropy shapes are highly oblate in all samples except UEK1-13C for AMS and all samples for AIRM, and weakly oblate for AARMs and ApIRMs (Fig. 4). Subsample UEK1-13C differs from the others in being from the sandy part of the outcrop that did not yield palaeomagnetic evidence. Remanence anisotropies are largely coaxial to one another and show a more distinct grouping of k_1 and k_2 axes than the AMS. The full AIRM, being a superposition of low- and high-coercivity grains shows larger spread than either the AARM or the ApIRMs. The observed differences between the AMS and remanence anisotropies can be explained by the presence of non-remanence-carrying grains such as para/diamagnetic minerals, and MD magnetite, as well as high-coercivity grains not targeted by the AIRM measured in a 1 T maximum field. Differences between AARM and ApIRMs reflect different anisotropy degrees of the low- and high-coercivity remanence carriers. As shown in Sect. 3.1, the low coercivity fraction may be composed from impure magnetite, while the high coercivity fraction of UEK and EGG is mainly represented by haematite. Note that

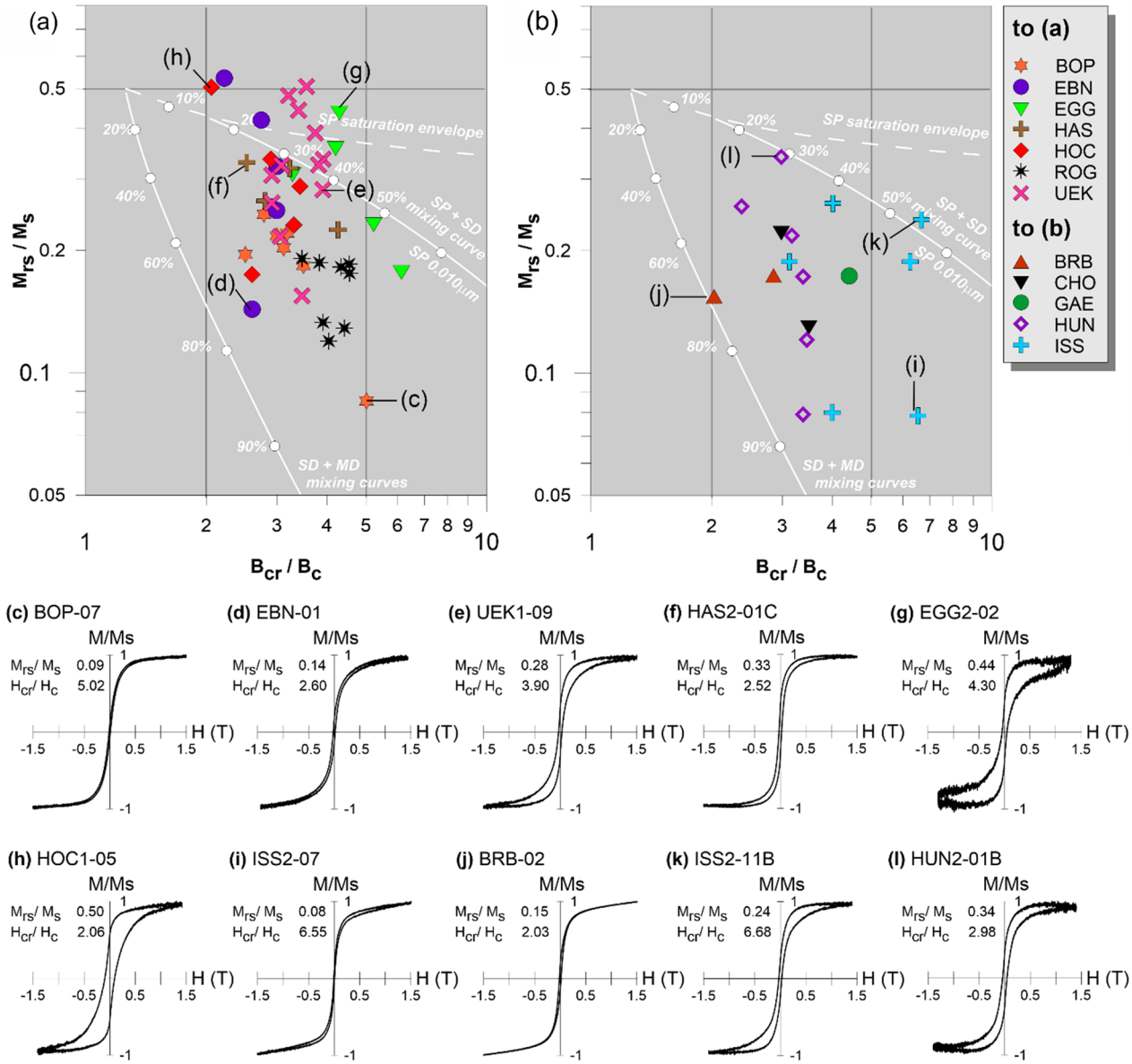

Fig. 3 Ratios of hysteresis parameters in Day plots (Day et al., 1977) for HDS (**a**) and TDS (**b**) and exemplary hysteresis loops (**c**-l). Mixing lines for (titano)magnetite are drawn after Dunlop (2002) (white lines) and only shown for comparison

the anisotropy of the low-coercivity fraction, is predominantly caused by shape and distribution anisotropy related to shape preferred orientation and arrangement of the grains, while haematite is controlled by magnetocrystalline anisotropy and crystallographic preferred orientation. Because the high-coercivity grains display the strongest anisotropies, the largest deviations in magnetisation directions and intensities are expected for the remanence carried by those particles. The occurrence of minimum principal axes perpendicular to bedding implies that the haematite must have been affected by compaction. This is only the case if the minerals are detrital or if they formed early in post-depositional history (Tan et al., 2002, Bilardello and Kodama, 2009). This makes it likely that the NRMs of the sub-samples examined contain detrital haematite, which, unlike authigenic haematite, is characterised by strong inclination shallowing (Tauxe and Kent, 1984, Bilardello and Kodama,

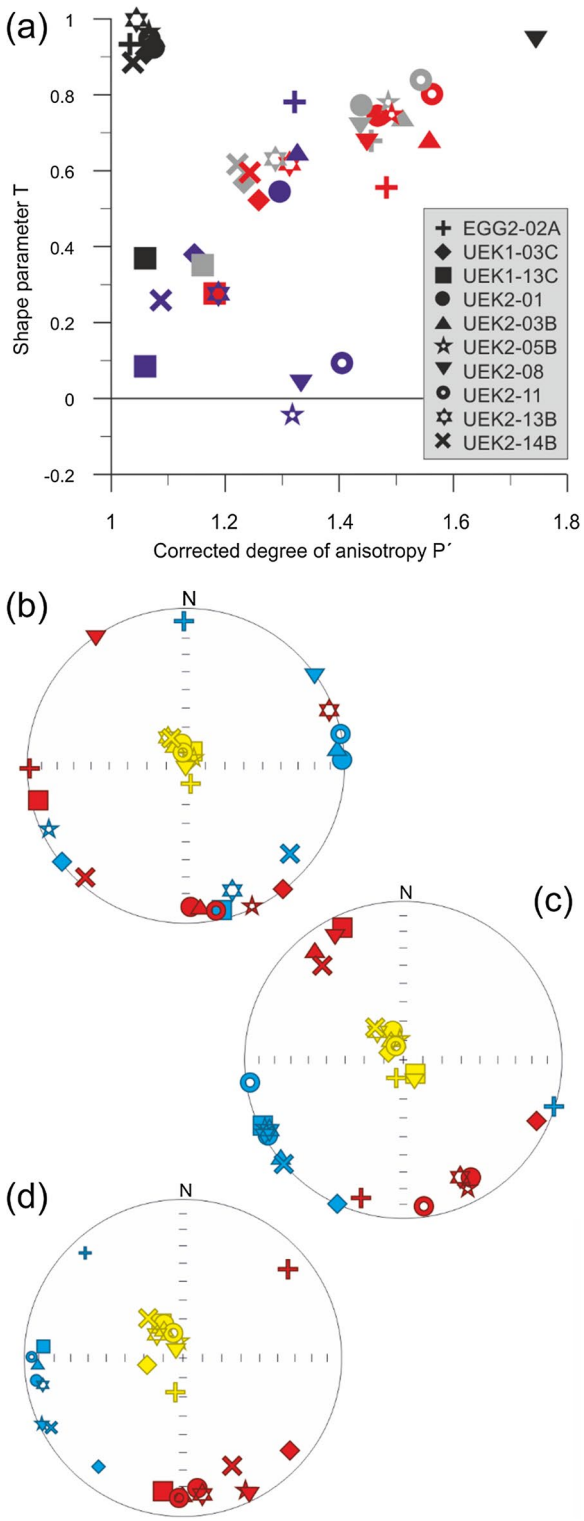

Fig. 4 AMS parameters and Lambert projections of the k_1, k_2, and k_3 axes of individual samples. **a** Jelinek plot showing the ARM (black), AARM (purple), $ApIRM_{100\,mT\text{-}1\,T}$ (grey), $ApIRM_{140\,mT\text{-}1\,T}$ (red). The axes k_1 (blue), k_2 (red), and k_3 (yellow) of AMS (**b**), AARM (**c**) and $ApIRM_{0.1-140}$ (**d**). $ApIRM_{0.1-100}$ is very similar to **d**. All individual values are provided in Additional file 1: Table S3 and by Scheidt et al. (2023)

2009). Contrary to ApIRM based anisotropy corrections AMS-based anisotropy corrections would under-correct the characteristic remanence data in this study. However, since any correction would add further uncertainties to the already difficult-to-interpret data, no correction of inclination was carried out in this study.

3.3 Magnetic polarity stratigraphy

Based on the mineral magnetic and AMS analyses, the subsamples in the final sample set are assumed to carry a DRM or a pDRM. The ChRM isolated from the 69 HDS subsamples indicate both, normal and reversed polarity, while the 21 TDS subsamples are exclusively normal (Fig. 5; Additional file 1: Table S2). Information to the subsamples of the individual sites are presented sorted by region. Please note that Zijderveld and demagnetisation diagrams are provided in the supplement.

3.3.1 Irchel Plateau

Four sites situated at the Irchel Plateau are investigated in this study. The samples of the HOC site are characterised by rather weak NRM with low thermal stability. Due to inconclusive directions, erratic demagnetisation paths and low thermal stability of the magnetisation (e.g., Additional file 1: Figs. S1, S2), the data of a large number of samples were discarded (Additional file 1: Table S2). The accepted samples show low directional consistency of the demagnetisation paths resulting in maximum angular deviation (MAD) values between 10.7° and 37.6° (Additional file 1: Table S2). The determined vectors indicate reversed polarity for all but the uppermost sample at the top of the ~ 2.5 m thick succession (Fig. 5; Table 3). This sample with normal polarity exhibited a reversed overprint (Additional file 1: Fig. S2e) that proves the sample to be deposited at a time of normal polarity of the EMF prior to the Brunhes Chron. A roughly antiparallel to the ChRM oriented secondary magnetisation is also recognised in three of the samples with reversed polarity. In general, the overprints are demagnetised in temperatures up to 255 °C (Additional file 1: Fig. S2). The blocking temperature spectra partly overlaps with that of the primary magnetisation. Ferrimagnetic sulphide minerals are no potential carriers of the secondary magnetisation at HOC as the magnetic susceptibility remain largely constant during thermal demagnetisation. Thus, a CRM carried by goethite or a VRM can be assumed. The results gained appear in general similar to those of Graf (1993). He describes a tendency towards inverse magnetisation for two of his samples while the remaining 17 samples showed discontinuous demagnetisation curves. Since Graf (1993) did not determine the ChRM and his raw measurement data have not been preserved, a thorough comparison to the results in this study is not possible.

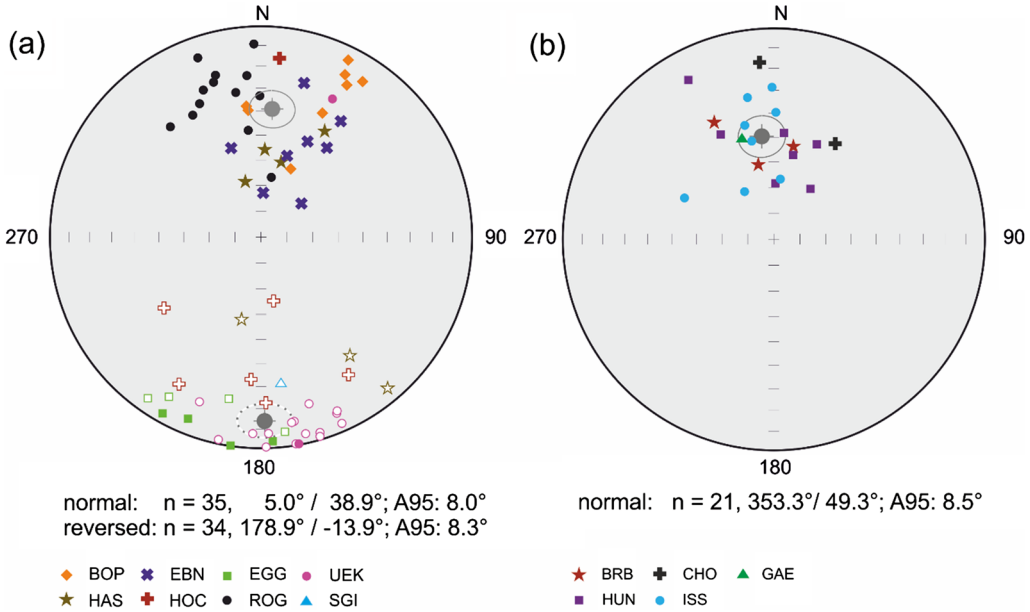

Fig. 5 ChRM distribution of all samples of HDS (**a**) and TDS (**b**) sites in Lambert projections. The open and filled symbols indicate upward and downward directions of the vectors, respectively (upward = negative inclination, downward = positive inclination). Mean direction are shown with the 95% confidence cone (A95) in grey

At EBN, eight samples from four depth levels of the sampled ~ 0.7 m thick layer yielded well-defined ChRM. The samples indicate exclusively normal polarity without showing antiparallel magnetisations. AF and TH demagnetised sister samples reveal very similar results (Additional file 1: Fig. S3b–e). Larger MAD (Table 3) are due to stable remanence values over several demagnetisation steps, resulting in a cluster of points around the same value in the Zijderveld diagram (e.g., Additional file 1: Fig. S3c, d). The identified ChRMs are suggested to reflect primary directions because magnetite and hematite, as the main carriers of remanence, indicate the same principal direction, and inclination shallowing can be detected. Only the lowest sample EBN-01 shows a gradual decreasing demagnetisation path over the entire temperature range, which could be due to authigenic haematite formation. Furthermore, four subsamples from two additional depth layers of the sequence did not give reliable results. The NRM intensity of these subsamples was lower and demagnetisation experiments showed inconsistent or unexpected (such as east–west running) vector directions (Additional file 1: Figs. S2, S3g, h). These samples may have been similar to those of Graf (1993), who could not find stable magnetisation for samples from the EBN site.

At SGI, the results of the palaeomagnetic analyses are similar to those of the HOC site. Due to erratic demagnetisation paths, low resistance to the demagnetisation process and conflicting inclination and declination directions, only one out of eight samples provided a ChRM. This sample, SGI-12 from the base of the ~ 1.8 m thick overbank deposits mapped as Hasli Fm, shows reversed magnetisation (Fig. 5; Table 3). An antiparallel overprint is erased with the 120 °C temperature step (Additional file 1: Fig. S4f). However, also within the discarded samples a tendency of reversed magnetisation directions can be observed (Additional file 1: Fig. S4a–e).

The samples from the HAS site were particularly difficult to interpret in terms of their magnetic polarity. As reported above, a decreasing trend of the NRM was observed, confirming the visual impression of a strong diagenetic overprint and questioning the primary origin of the recorded magnetic directions. In the lower 4.33 m of the ~ 6.2 m thick sediment profile, AF demagnetisation had only little effect, while thermal demagnetisation removed significant parts of the magnetisation by the 120 °C step and the rest by the 350 °C step at the latest. As a consequence of the dominance of goethite, the data of all AF demagnetised samples were called into question and discarded although some carried a stable signal. Overall, from the lower part of the sediment only sample HAS2-13 from 0.77 m above the underlying gravel yielded a ChRM. It indicates reversed polarity and shows a normal overprint (Additional file 1: Fig. S5k). Above, only samples from between 4.36 m and 5.51 m allowed to determine the ChRM. Accordingly, sample HAS1-03 from 4.36 m indicates normal polarity, while samples HAS1-02 and HAS1-01 from 4.44 m

Table 3 Overview on the numbers of samples taken at the sites of individual regions and the summarised results of magnetic stratigraphy

	Site	Unit	Magnetic stratigraphy results[a]	Mean direction (declination/inclination)	Comments
Irchel Plateau	EBN	HDS	Normal (8/4) Discarded (5)	21.2°/52.2° (n = 8; A95: 14.3°)	No antiparallel directions MAD range: 6.8°–21.3 °C
	HAS	HDS	Normal (4/4) Reversed (3/3) Discarded (23)	12.1°/57.2° (n = 4; A95 = 17.8°) 152.5°/-33.5° (n = 3; A95 = 54.8°)	Difficult to interpret Once an antiparallel direction MAD range: 9.9°–18.3°
	HOC	HDS	Normal (1/1) Reversed (6/4) Discarded (16)	5.9°/ 15.8° (MAD = 11.8°) 186.9°/-37.8° (n = 6; A95 = 25.8°)	Antiparallel directions MAD range: 10.5°–37.6°
	SGI	HDS	Reversed (1/1) Discarded (7)	172.3°/-30.6° (MAD: 14.2°)	Antiparallel directions
Albis Ridge	BUE	HDS	Discarded (5)	#	No primary magnetisation preserved
	UEK	HDS	Normal (1/1) Reversed (14/10) Discarded (16)	27.3°/27.1° (MAD: 16.4°) 171.1°/–7.4° (A95: 6.3°)	No antiparallel directions MAD range: 1.5°–16.4°
Dürn-Gländ-Egg	TRO	HDS	Discarded (5)	#	Not analysed
	EGG	HDS	Reversed (8/7) Discarded (3)	–4.5°/195.7° (A95: 13.3°)	Overprints not antiparallel MAD range:5.4°–18.3°
	BOP	HDS	Normal (8/8) Discarded (2)	20.3°/28.8° (A95:15.9°)	Once an antiparallel direction MAD range: 1.3°–23.4°
	FEU	HDS	Discarded (7)	#	No primary magnetisation preserved
Lower Aare Valley	ROG	HDS[a]	Normal (13/10) Discarded (9)	345.1°/ 30.6° (A95: 9.5°)	No antiparallel directions MAD range: 6.9°–24.1°
	GAE	TDS	Normal (1/1) Discarded (1)	342. 3°/ 48.8° (MAD:16.8°)	Only one sample No antiparallel directions
	ISS	TDS	Normal (8/6) Discarded (6)	346.0°/49.4° (A95: 14.3°)	No antiparallel directions MAD range: 10.2°–27.8°
	BRB	TDS	Normal (3/2) Discarded (1)	349.4°/ 51.4° (A95: 26.6°)	No antiparallel directions MAD range: 7.4°–21.3°
Lake Constance-Schaffhausen	CHO	TDS	Normal (2/2) Discarded (2)	11.1°/ 32.4° (A95: 110.5°)	No antiparallel directions MAD range: 18.0°–25.9°
	HUN	TDS	Normal (7/6) Discarded (40)	258.9°/ 52.1° (A95:18.1°)	No antiparallel directions MAD range: 6.8°–23.0°

[a] The numbers in brackets indicate the number of subsamples to which the result applies and the number of depth levels that are represented (e.g., 8/6 means 8 samples from 6 different depth level)

and 4.55 m, respectively, show reversed polarity. Above, samples from 4.83 m, 5.16 m, and 5.51 m indicate again normal polarity (Additional file 1: Fig. S5). This sequence of observed polarities (from bottom to top: reversed—normal—reversed—normal) does not seem to reflect a realistic record of the EMF's polarity swings, as fluvial overbank deposition over a period of several subchrons is unlikely in an uplift-influenced area. Thus, one or more samples must give false results. A likely candidate is HAS1-03, in which a redox front runs across the sample separating an orange-brown and a grey-green area (Additional file 1: Fig. S5a). Due to the possible associated overprinting, the sample should only be included in the polarity stratigraphy with reservation. Alternatively, subsamples HAS1-02 and HAS1-01 could also give false results of reversed polarity. The magnetisation of these samples is already reduced by 60 to 70% at the 160 °C temperature step, indicating a distinct secondary component of the NRM. In addition, the indicated directions of these samples appear rather twisted, as they lie at the outer margin of the distribution of the reversed ChRMs of the HDS (Fig. 5). However, despite the vertical distance of 11 cm, the ChRMs of these two samples confirm each other by the similarity of their directions. Furthermore, the reversed signals have been retained at least over the time of the Brunhes Chron, which cannot be stated with certainty about sample HAS1-03. Therefore, we tentatively exclude HAS1-03 which would result in a sequence with inverse directions at the bottom and normal directions at the top. Despite the high directional stability of

the three upper samples the primary origin of their normal polarity signals is also not clear, because the ChRM inclination of these samples is only slightly flatter than that of the present EMF and the demagnetisation paths are characterised by a gradual decrease. As described in Sect. 3.1, this can be interpreted as a signal carried by authigenic haematite, which may have formed long after deposition of the sediment. In contrast to the results presented in this study, Bolliger et al. (1996) reported results from 11 out of 20 samples from a 4 m long profile at the HAS site. They found that eight of the samples showed a normal magnetisation, whereby five of them carried a reversed overprint. Since the depth from which their samples were taken is not documented and no demagnetisation diagrams or Zijderveld diagrams are shown, no conclusions can be drawn as to the reasons for the differences between their results and those of this study.

3.3.2 Albis Ridge

The Albis Ridge region comprises two sites, BUE and UEK. From BUE, no samples were used for magnetic polarity stratigraphy, as demagnetisation behaviour (blocking temperatures, GRM acquisition) indicated the dominance of secondarily formed sulphide minerals (Table 3; Additional file 1: Fig. S6), which are unlikely to carry a pDRM. This is consistent to the findings of Graf (2019), who reports palaeomagnetic analyses on samples from a profile named Albis-2 that corresponds to the BUE site in this study. In that study, the samples were also interpreted to carry a CRM showing normal polarity.

In contrast to BUE, 15 samples from 11 depth levels of the 2.5 m thick sequence at the UEK site yielded palaeomagnetic directions (Table 3). These samples are from a ~ 0.7 m thick silty to clayey sediment layer located between more sandy sections in the upper and lower parts of the outcrop (Additional file 1: Fig. S7). Due to inconsistent, unstable, or ambiguous magnetisation directions, the sample data from the sandy sections were completely excluded from this study. The samples considered are mainly characterised by very stable and consistent vector directions over all demagnetisation steps. Antiparallel overprints were generally not encountered. In all samples except UEK1-03A, a reversed polarity is mainly carried by the thermally very stable mineral haematite. In a contrasting way, sample UEK1-03A from the upper part of the silty to clayey section lost about 70% of its magnetisation already at 200 °C and shows a gradual decrease of the remaining magnetisation with the higher temperature steps (single line vs. general trend in Fig. 2d). Since subsample UEK1-03A differs from the other samples in the carriers of the magnetisation and at the same time is the only one indicating a normal position of the EMF, this result should be treated with caution. The completely different vector directions determined from sample UEK1-03A's AF demagnetised sister sample UEK1-03B additionally advises to be careful (Additional file 1: Fig. S7). Therefore, only the reversed polarity in the outcrop can be confirmed with certainty in this study. This result somewhat contradicts Graf's (2019) findings at the UEK site. One factor here is the different assessment of the data. Graf (2019) reports on normal but also reverse magnetised sediments and describes a westward deviation of several of his samples that he attributes to mechanical overprinting by glaciers. By contrast, this study excluded all data from samples that may have been affected by mechanical overprinting. This include samples with East–West running vectors but also some samples with contradicting inclination and declination orientations. We suggest these findings could be due to undetected deformation in the sampled layers, as water escape cusps and convoluted bedding were locally detected in surrounding areas. However, it could also be related to mineral rotation and/or the formation of new minerals in pore spaces, as well as completely different processes. The occurrence of this roughly east–west oriented vector is noteworthy as it also occurs in different subsamples from other outcrops as secondary overprint or ChRM (see supplement)). However, the cause of these conspicuous east–west directions is not conclusively analysed in this study nor in that of Graf (2019), as this would have required more detailed AMS measurements (e.g., Fleming et al., 2013), which would not have fitted into the scope of the two studies. Another aspect in which this study diverge from the interpretation of Graf (2019) is the origin of the haematite that is identified as an important carrier of the remanence in both studies. While Graf (2019) interpret the haematite as authigenic formation, this study suggest a detrital origin because (a) the inclination values are shallow (Tauxe and Kent, 1984), (b) the samples show a sudden drop at the T_N of haematite and no gradual decrease (Jiang et al., 2022), and (c) with a few exceptions, there is a small but consistent gradual change in declination values within the profile (Additional file 1: Table S2), that might result from little changes of the EMF direction during the successive deposition of the sediments.

3.3.3 Dürn–Gländ–Egg

The HDS sites TRO, EGG, BOP and FEU are grouped together as Dürn–Gländ–Egg region. The only sample of the HDS site TRO was not processed because the sample, which appeared well compacted when collected, disintegrated during preparation due to the lack of binders (Additional file 1: Fig. S8).

The samples from the two thin layers (< 0.5 m; Additional file 1: Fig. S9) from the EGG site revealed a

reversed magnetisation characterised by very shallow inclination values (Table 3). The remanence is mainly carried by haematite, as indicated by resistance against AF demagnetisation and high thermal stability (Fig. 2b, e). This is in line with the results of Graf (1993), who also identified large contributions of haematite and determined mean declination and inclination value of 192.4° and −12.6°, respectively. Graf (1993), however, describes secondary magnetisations oriented antiparallel to the ChRM. In this study, secondary magnetisations were found only in two subsamples; in one case with a slight angle to the ChRM and in the other subsample with an east–west orientation (Additional file 1: Fig. S9).

The samples from BOP originate from fine-grained silty to fine-sandy intercalations in a gravel sequence several metres thick. In contrast to EGG, all samples of the BOP site yield normal ChRM which are mostly well defined (Table 3). Only one sample (BOP-04B) shows an overprint. This overprint is demagnetised with the 120 °C stage and is therefore probably carried by goethite (Additional file 1: Fig. S10). Due to the carrier mineral and the rather westward vector of this overprinting, it likely represents just a preferential direction given by e.g. pore space. The relatively high NRM values of all BOP samples suggest that no waterlogging and associated reductive conditions influenced the sediments. Similar to EGG, haematite is an important part of the magnetic mineralogy, though supplemented by magnetite in variable portions (Additional file 1: Fig. S10). The presence of haematite likely causes the rather low inclination values of the ChRM (Fig. 5).

The data of the relative coarse sediments of the FEU site had to be discarded completely, as they showed contradicting inclination and declination or were demagnetised in low AF fields or by low temperatures (Additional file 1: Fig. S11).

3.3.4 Lower Aare Valley

The Lower Aare Valley region comprises the sites ROG, GAE, ISS, and BRB. From these sites ROG is the only one attributed to the HDS. At ROG, two different stratigraphic levels were sampled. While the samples from the upper, sandy section did not reveal stable demagnetisation paths, all but one sample of the lower, ~ 1.1 m thick fine sandy to clayey silt layer yielded stable ChRM. Directional consistency is also observed when comparing AF and TH demagnetised sister samples (Additional file 1: Fig. S12). The relative high MAD values observed (Table 3) result from the large portions of high coercivity minerals (Fig. 2) that cause clustering of magnetisation values in the Zijderveld diagram (Additional file 1: Fig. S12). It is noteworthy, that the normal results of ROG are associated with N to NW pointing vectors, which fit better to the distribution of the TDS than to the normal results of the HDS (Table 3; Fig. 5). Excluding the ROG samples would change the mean declination and inclination directions of the normal subsamples of HDS to 18.9°/42° (n = 22; A95: 9.2°).

Two samples were taken from the TDS site GAE, of which only the AF demagnetised sample GAE-01 was considered in the final sample set. The TH demagnetised sample GAE-02 showed an unexpected direction, which is probably due to disturbed bedding of the layers. Nevertheless, GAE-02 tendentially indicates normal polarity (Additional file 1: Fig. S13). GAE-01 retained 31% of the NRM after the peak AF field of 300 mT was reached and show a scattered demagnetisation path. PCA using the steps 15–80 mT and 100–300 mT result in ChRM estimates of 349.2°/63.7° (MAD: 16.7°) and 341.7°/38° (MAD: 19.3°), respectively. Thus, the high coercivity component shows a shallower inclination, which is expected for detrital haematite. Accordingly, it is assumed that the ChRM provides reliable information about the normal polarity during time of deposition (Fig. 5).

At the ISS site, samples originate from finer intercalations within a ~ 35 m thick gravel section (Additional file 1: Fig. S14). The samples had to be discarded frequently due to a large number of insect burrows inside, though the sediment surface was cleaned as good as possible. The samples also indicate only normal polarity (Fig. 5) without antiparallel overprints. As mentioned before, high MAD values (Table 3) result from samples dominated by high coercivity minerals (Additional file 1: Fig. S14). AF demagnetised subsamples usually show steeper inclination values than TH demagnetised sister samples (Additional file 1: Fig. S14). This phenomenon is likely due to goethite, which is TH demagnetised at 120 °C but continuously superimposes the magnetisation of AF demagnetised samples. When AF demagnetised subsamples are excluded, a mean declination/inclination of 345.7°/42.9° (A95: 16.2, n = 6) is obtained (c.f., Table 3). The directions of the TH demagnetised sample ISS2-04 appear to be slightly rotated compared to the other samples. If this sample is also excluded, a narrower distribution (A95: 9.8°, n = 5) remains with mean declination and inclination values of 352.9° and 39.1°, respectively.

The samples from the TDS site BRB were taken from individual, up to 0.4 m thick sandy layers within a ~ 10 m thick gravel section. Due to an insignificant portion of high-coercivity minerals, the samples were only AF demagnetised (Fig. 2). The subsamples of sample BRB-04 showed inconsistent NRM among each other and were therefore not further processed. Three subsamples from two outcrops of the BRB site indicate exclusively normal polarity with no antiparallel secondary magnetisation overprints (Fig. 5; Additional file 1: Fig. S15; Table 3). The

large values of the individual MADs of the subsamples of the BRB site are not associated with high coercivity minerals but with scatter in demagnetisation paths.

3.3.5 Lake Constance–Schaffhausen

Within the region Lake Constance–Schaffhausen the sites CHO and HUN were investigated. At CHO only the samples from the around 0.4 m thick upper of the two sampled stratigraphic levels yield results (Additional file 1: Fig. S16). Samples showed normal polarity ChRM and no secondary overprints (Fig. 5; Table 3). The discarded samples also indicated a normal direction of the EMF, but were not considered as they were largely demagnetised at 400 °C.

Special attention was paid to site HUN, as it is the only known relatively long profile of the TDS composed of dominantly fine-grained sediments. The profile is divided into a lower and an upper part by a thin gravel layer. Overall, the abundance of iron oxide and manganese precipitation horizons (Additional file 1: Fig. S17) indicates fluctuating groundwater levels at this site over time. As a result of associated reductive diagenesis, NRM decreases downward and most samples did not carry a reliable magnetic signal (Table 3). The rejection of samples was based on erratic demagnetisation patterns and contradictory or misoriented vector directions. The seven samples from six depths level providing reliable ChRMs are distributed over the entire, around 6.5 m thick profile with vertical distances between 3 and 140 cm to each other. All samples acquired remanence during times of normal polarity of the EMF (Fig. 5; Additional file 1: Table S2). Antiparallel overprints were not encountered. However, the ChRM of the samples from the upper part of the outcrop are oriented slightly to the Northeast, while the ChRM of the samples from the lower part are oriented to the North to Northwest (Fig. 5).

4 Age constraints derived from palaeomagnetic investigations

In palaeomagnetic studies, it is of enormous importance to ensure that the ChRM of a sample reflecting the direction of the EMF at time of deposition or shortly after (DRM or pDRM), and not a CRM, that could be acquired any time later. The selection procedure implemented in this study lead to determination of a consistent dataset for the deposits of the HDS and TDS sites investigated (Fig. 6).

4.1 Irchel Plateau

From all sites investigated at Irchel Plateau, only the ChRMs of the HAS site are somewhat uncertain. As presented above, this study tentatively suggests to exclude sample HAS1-03 to receive a pattern of reversed polarity in the lower and normal polarity in the upper part of the HAS profile (Fig. 6). However, even the alternative exclusion of HAS1-01 and HAS1-03 would result in the same overall picture. Thus, the sediments at HAS and HOC both show reversed magnetisation in the lower part and normal magnetisation in the upper part of the respective profiles. The sampled layers at the HAS, HOC and SGI sites are assumed to all belong to the fine-grained sediments of the Hasli Formation (Hasli Fm) at Irchel and are likely to represent interconnected overbank deposits formed during the same period in the Quaternary (Graf, 1993; Preusser et al., 2011). Accordingly, the single subsample from the base of the SGI site would represent the time of reversed polarity before the reversal. With the palaeomagnetic information alone, the age of the Hasli-Fm at HOC, HAS and SGI can be constrained to > 1.008 Ma, as subchron C1r.1n (Jaramillo; Fig. 7) is the last time at which sample HOC2-06 could acquire a normal ChRM which has later been reversed overprinted. However, the Hasli Fm is a temperate climate deposit with its age already delimited by Bolliger et al. (1996). They identified a mammalian assemblage from the mammalian fauna biozone MN 17 (2.6–1.8 Ma; Fejfar & Heinrich, 1990) in a layer just below sample HAS1-03 (Fig. 6). Cuenca-Bescós (2015) reanalysed the faunal assemblage of the Irchel and found indications for a correlation with the late MN17 corresponding to a time interval of about 1.8–2 Ma. These biostratigraphic results combined with the palaeomagnetic information obtained in this study indicate that the Hasli Fm at HAS and HOC was accumulated during the transition into the C2n (Olduvai) subchron at 1.934 Ma and includes the warm period in MIS 71 (Fig. 7) (Lisiecki and Raymo, 2005; Raffi et al., 2020). A correlation with the long interglacial MIS81 (Lisiecki and Raymo, 2005) and subchron C2r.1n (recently renamed Feni, previously Réunion) at 2.155 Ma (Raffi et al., 2020) as suggested by Kuhlemann and Rahn (2013) seems less likely, as it would contradict the narrower biostratigraphic zone proposed by Cuenca-Bescós (2015). Additionally, subchron C2r.1n (Feni) is hardly documented in any continental sedimentary archive (Channell et al., 2020) and is thus, not likely to be found at Irchel or elsewhere in the Deckenschotter.

The overall picture of the Irchel Plateau presented so far is currently being challenged by the dating results of studies using $^{26}Al/^{10}Be$ isochron-burial dating and ^{10}Be depth-profile dating (Akçar et al., 2017; Claude et al., 2019; Dieleman et al., 2022; Knudsen et al., 2020). These studies, in combination, suggest that the deposition ages for the Deckenschotter unit cluster around 1, 1.5 and 2.5 Ma with a relatively constant regional base level. At the Irchel Plateau, burial ages derived from the

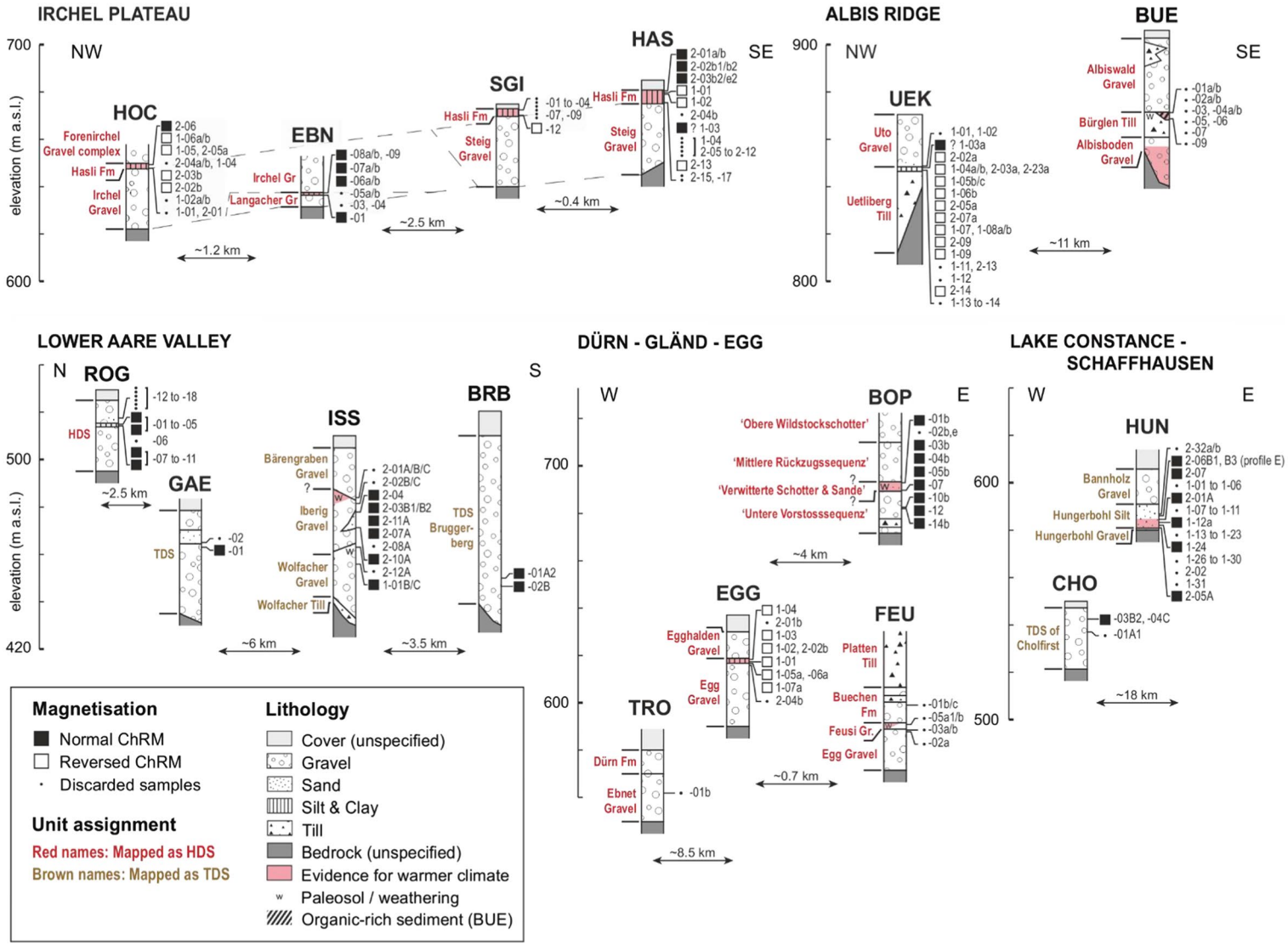

Fig. 6 Overview on the magnetic stratigraphy results within lithological profiles of the sites. Formation names according to www.strati.ch (2022). Informal names are indicated by quotation marks. Stratigraphic correlation only for Irchel. The sedimentological profiles are based on our own data, which are supplemented with information from the following sources: Irchel Plateau: Bolliger et al. (1996), Graf (1996), Preusser et al. (2011), Haldimann et al. (2017). Albis Ridge: Pavoni et al. (1992), Gubler (1996), Gubler (2009), Graf (2019). Lower Aare valley: Graf (1993), Matousek et al. (2000), Diebold et al. (2005), Preusser et al. (2011). ISS shows a summary log displaying the main features of the outcrop and drill core data. Dürn–Gländ–Egg: Güller (1944), Graf (1993), Bitterli-Dreher et al. (2007), Graf (2009), Haldimann et al. (2017). Lake Constance–Schaffhausen: Hofmann and Hantke (1964), Zaugg et al. (2008), Graf (2009)

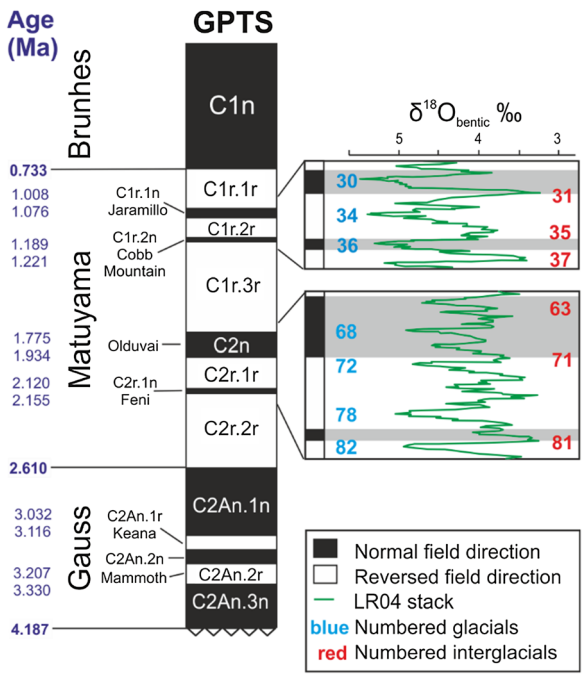

Fig. 7 Times of geomagnetic polarity changes as shown in the Astronomically Tuned Neogene Time Scale ATNTS2020 (Raffi et al., 2020). The LR04 oxygen isotope fractionation curve and corresponding marine isotope stages (Lisiecki and Raymo, 2005) provide indications on warmer periods

gravels below the Hasli Fm are partly in disagreement with the biostratigraphic evidence for MN17. Therefore, Claude et al. (2019) and Dieleman et al. (2022) propose a laterally discontinuous stratigraphy resulting from cut-and-fill processes. However, this hypothesis cannot explain the apparent age inversion at the HAS site, which results from the biostratigraphic classification to MN17 (Bolliger et al., 1996; Cuenca-Bescós, 2015) compared with an age of 1.3 ± 0.1 Ma determined at a gravel layer approximately 10 m below our HAS site (Dieleman et al., 2022). If the age of Dieleman et al. (2022) is correct, the pattern of normal followed by reversed magnetisation at HAS would suggest deposition either around the transition of the C1r.3r to C1r.2n (1.22 Ma) or C1r.2r to C1r.1n (1.076 Ma) subchrons. A reinterpretation of the palaeomagnetic results is also required at site SGI if the isochron burial age of 0.9 ± 0.4 Ma Claude et al. (2019) of Steig gravels below the Hasli Fm at our SGI site is considered. The single sample showing reversed magnetisation could only have acquired its remanence during magnetochrons C1r.1r (1.008–0.773 Ma), C1r.2r (1.221–1.189 Ma), or during the late C1r.3r (1.775–1.221 Ma). However, Knudsen et al. (2020) recalculated the dating result of Claude et al. (2019) and determined a younger age of 0.69 ± 0.25 Ma (P-PINI model) or a similar age of 0.9 ± 0.17 Ma (Bayesian model). The younger result would limit the possible remanence acquisition time to subchron C1r.1r. In contrast, the cosmogenic nuclide dating results do not affect the palaeomagnetic interpretation of site HOC, as Dieleman et al. (2022) determined an age of 2.6 ± 0.1 Ma for the gravels underlying the Hasli Fm at the HOC site. This dating result supports a depositional period around the transition from subchron C2r.1r to C2n (1.934 Ma), if biostratigraphic results are transferred to HOC. Finally, Dieleman et al. (2022) also put the results of the site EBN in a different light. Before this study was published, the deposits at EBN were regarded as the oldest deposit at Irchel (Claude et al., 2019; Graf, 1993, 1996). The sediment petrographic characteristics were interpreted as deposits of a warm period prior to deposition of the Hasli Fm (Graf, 1993). Based on this knowledge, the normally magnetised samples would probably have been interpreted as of Gaussian age (> 2.61 Ma; Fig. 7), as preservation of subchron C2r.1n in fluvial sediments seems very unlikely (Channell et al., 2020). However, Dieleman et al. (2022) report an age of 1.3 ± 0.1 Ma for the Schartenfluh site which is stratigraphically equivalent to the crystalline-rich basal Langacher Gravel (Haldimann et al., 2017) underlying the overbank deposits sampled at site EBN (Fig. 6). Taking this age information into account, the samples could have been magnetised during normal polarity in any period. Since no antiparallel overprints were detected, even the Brunhes Chron cannot be ruled out. Overall, the question remains open as to how the various dating results from the Irchel Plateau can be meaningfully combined in a plausible stratigraphic model. As Knudsen et al. (2020) demonstrated how assumptions can change the cosmogenic nuclide dates clearly, our new palaeomagnetic evidence may help subsequent studies to adjust dating procedures.

4.2 Albis Ridge

In contrast to the Irchel, no cosmogenic nuclide dating is available for the Albis Ridge region. Thus, only the results of Graf (2019) and this study (Fig. 6) are recently available to provide age constraints for the investigated HDS sites. Magnetic polarity stratigraphy clearly indicates a deposition of the silts and sands between the Uetliberg Till and the Uto Gravel during times of a reversed geomagnetic field, and thus, during the Matuyama Chron (Fig. 7). A further delimitation of the age is only possible if the top, normal magnetised subsample provided by this study is included in the analysis, though it should only be used

with extreme caution. However, if it is considered for magnetic polarity stratigraphy the deposition of HDS at UEK can be constrained to any time of transition from reversed to normal polarity (Fig. 7).

4.3 Dürn–Gländ–Egg

At the HDS site EGG in region Dürn–Gländ–Egg all samples show reversed polarity (Fig. 6) and can thus, be attributed to any time of reversed polarity of the Matuyama Chron (Fig. 7). While no cosmogenic burial ages are available from the EGG site, Knudsen et al. (2020) report a P-PINI age of 0.93 ± 0.13 Ma for the glacigenic diamicts within the Buechen Fm at the nearby gravel pit Feusi (FEU, Fig. 6), where–in turn–no palaeomagnetic results could be obtained. Graf (1993) suggested to correlate weathered sediments on the top of the Feusi Gravel at site FEU (i.e. below the stratigraphic level of the cosmogenic burial date at Feusi) with the interglacial overbank deposits in the top of the Egg Gravel at site EGG. Thus, the reversed polarity at EGG is likely to have been acquired in the Matuyama Chron prior to 0.93 ± 0.13 Ma (Fig. 7). A similar comparison was attempted at the TRO site, where Knudsen et al. (2020) reported a P-PINI age of 0.88 ± 0.14 Ma but unfortunately the paleomagnetic sample from this site did not yield results.

If the assignment of BOP to HDS is accepted and it is assumed that the HDS of BOP were deposited in a similar period as e.g. the HDS at Irchel Plateau, an age older than 0.773 Ma (C1n; Fig. 7) becomes likely. Accordingly, the normal ChRM at BOP (Fig. 6) would likely refer to the subchrons C2n (Olduvai; 1.775–1.934 Ma) or C1r.1n (Jaramillo, 1.008–1.076 Ma). However, because no antiparallel overprints were detected, magnetic polarity stratigraphy cannot provide clear evidence for an age > 0.773 Ma. Only the determined ChRMs can be considered. They point towards Northeast, as those of EBN and not to North to Northwest as those of the majority of the TDS sites (Fig. 5).

4.4 Lower Aare Valley and Lake Constance–Schaffhausen

In the regions Lower Aare Valley and Lake Constance–Schaffhausen, exclusively normal ChRM were obtained, although the investigated sites are associated with the HDS (ROG) and the TDS (GAE, ISS, BRB, HUN,CHO) (Fig. 6; Graf, 1993). For some of the sites cosmogenic nuclide ages are available. The single normal ChRM from GAE is in agreement with the 0.7 + 0.6/−0.3 Ma reported for the sands just above our sampling site (Claude et al., 2019). Knudsen et al. (2020) determined two different isochron burial ages for ISS from the same ^{10}Be and ^{26}Al measurements using the P-PINI model with and without Bayesian modelling. The palaeomagnetic evidence rather supports the younger of these ages (0.69 ± 0.12 Ma), as the older one (0.93 ± 0.17 Ma) overlaps only slightly with times of normal polarity of the EMF (Fig. 7). Cosmogenic nuclide dating was also applied to the HDS-attributed site Mandach (Akçar et al., 2014, 2017), which is located ~ 2.8 km south-southeast of ROG and attributed to the same general HDS unit (Diebold et al., 2005; Graf, 1993). The exposure age of 1.02 ± 0.2 Ma gained by ^{10}Be depth-profile dating is interpreted by Akçar et al. (2014) and Akçar et al. (2017) to reflect the end of HDS-related glaciations in the Swiss Alps. The HDS depth profile data from Mandach (Akçar et al., 2014) was later remodelled by Claude et al. (2019) who report a much broader range of uncertainty of 0.8 + 1.4/−0.4 Ma for the Mandach site and it was left open whether the age represents a depositional age or the age of the exposure and onset of incision. If this age would apply to ROG as well, the sampled sediments could have acquired their magnetisation during the magnetochron C1r.1n (Jaramillo, 1.076–1.008 Ma) or C1n (Brunhes, < 0.733) (Raffi et al., 2020). We propose to assign the ROG site a maximum age of 0.733 Ma (magnetochron C1n, Brunhes) as the determined ChRM at ROG are Northwest pointing as those of the TDS sites investigated. Furthermore, no antiparallel overprint was detected. Thus, and despite its high topographic position (> 500 m a.s.l.), the ROG site could be attributed to TDS or the HT. The gravel foreset beds with the common syndepositional small-scale faults at the site could be re-interpreted as delta deposits into a rapidly aggrading lake dammed by a high-lying glacier margin. The required dam height could be reached in the event of an extensive Middle Pleistocene glaciation of the lower Aare Valley into the Hochrheine Valley.

The maximum age of 0.733 Ma can also be assumed to all other investigated TDS sites of the Lower Aare Valley and Constance-Schaffhausen region, as only normal magnetisations were encountered with no signs of antiparallel secondary overprints. However, the absence of overprinting is not a clear indication, as the sequence of polarity changes is only recorded by sediments under certain conditions. Doubts could also arise from the direction of the ChRM, as the upper part of HUN profile shows Northeast oriented ChRM like EBN and BOP. However, this could also be due to neotectonic activities or slope movements. Overall, magnetic polarity stratigraphy cannot exclude a deposition during times of normal polarity > 0.733 Ma. Nevertheless, palaeomagnetic studies of TDS deposits are rare. While Graf (1993) did not yield palaeomagnetic evidence for TDS sites in Switzerland, Rolf et al. (2012) summarised the outcome of unpublished studies of K. Fromm from the 1980ies and report on reversed polarity of Mindel-Deckenschotter in southern Upper Swabia, Germany, which could be temporal equivalents of the TDS in Northern Switzerland

(Ellwanger et al., 2011). A study in Allschwil showing reversed ChRM of TDS, as mentioned in the publications of Claude et al. (2017), was never published. The information is based only on a written communication from T. Forster of ETH Zurich, mentioned in Zollinger (1991). The application of magnetic polarity stratigraphy to further deposits of the TDS would be a tool to distinguish between Brunhes and Matuyama temporal deposits. In combination with biostratigraphy or cosmogenic nuclide dating, the method is likely to provide valuable insights into the age of the TDS.

5 Conclusions

Paleomagnetic analyses are challenging in the Deckenschotter, because of the sparse and fragmentary occurrence of suitable fine-grained sediment and frequently appearing overprints that can completely destroy the DRM or pDRM. We present a systematic workflow applicable to this methodologically unfavourable outcrop situation, including sampling procedure, characterisation of the magnetic properties and systematic acceptance criteria for magnetic polarity stratigraphy. The resulting consistent and reliable palaeomagnetic data set provides independent cross-checks for other dating methods.

Samples from eight HDS sites show both reversed and normal polarity. However, the interpretation of some of these sites is limited by the occurrence of the respective polarity according to the polarity time scale, as supplementary findings from other dating methods are missing to date. However, specific statements can be made for some sites.

- At the Irchel plateau (sites HAS, HOC, SGI, EBN), conflicting chronological of cosmogenic nuclide dating and biostratigraphic results allow for several interpretation schemes of the palaeomagnetic evidence. The palaeomagnetic evidence combined with the biostratigraphic results (Bolliger et al., 1996) suggest that the Hasli Fm was deposited during the transition into the C2n subchron (Olduvai, at 1.934 Ma). However, considering recent results of cosmogenic nuclide dating (Claude et al., 2019; Dieleman et al., 2022) the Hasli Fm could also acquire its remanence during earlier transition from normal to reversed polarity. Further evidence is needed to solve the question on the age of the Hasli Fm at the Irchel Plateau. The age of EBN at Irchel cannot be constrained to a single period of time. Depending on the applied stratigraphic model, the normally magnetised samples of the EBN may have Gaussian ages (> 2.610 Ma) or may have acquired their remanence in a normal subchron during the Matuyama chron (1.076–1.008 Ma; 1.221–1.189 Ma; 1.934–1.775 Ma, assuming that the Feni Subchron is unlikely to be recorded in fluvial sediments).
- Detailed characterisation at UEK reveal that the haematite is detrital and not in-situ formed as suggested by Graf (2019). Thus, we suggest the indicated reversed polarity to be primary.
- The site ROG is a special case as it is mapped as HDS but shows normal ChRM with orientations more similar to the investigated TDS sites as the other HDS sites. Thus, we suggest to reassign this site to the TDS or even HT.

TDS sites revealed only normal polarity, suggesting remanence acquisition during the Brunhes Chron (< 0.733 Ma). However, older periods with normal magnetisation cannot be ruled out based on the magnetic stratigraphy alone.

Overall the present study provides additional constraints for Early Pleistocene deposits of the Northern Alpine foreland and thus, important contributions towards a better understanding of the Quaternary landscape evolution of this region.

Supplementary Information

The online version contains supplementary material available at https://doi.org/10.1186/s00015-023-00439-y.

Additional file 1. The supporting material comprises information on the measurement procedures for the individual devices used at the different facilities, explanations of the naming scheme for the samples and detailed information on all sites investigated in this study. Sample lists with the individual measurement results are also provided.

Acknowledgements

We like to thank Daniel Kälin, Nigel Thew, and René Löpfe for allowing us to use a simplified version of their detailed description of the sedimentological profiles, as indicated in the supplementary material. We want to thank Thomas Gubler for a literature review and outcrop screening in the preparations to this study. We like to acknowledge Wildnispark Zürich and the Canton of Zurich for the permission to access the BUE outcrops located in protected areas.

Author contributions

GD initiated the study and suggested the sites. SS, GD and MB performed sampling. SS designed the methodological approach and prepared all the subsamples. RE designed software tools for data analyses. SS conducted all measurements and analysed and interpreted the data, except for the AMS, which was carried out by AB. SS coordinated the work at the manuscript. All authors contributed to the writing of the manuscript. SS and MB designed the figures. SS, GD, MB, and RE reviewed and edited the manuscript.

Funding

Open Access funding enabled and organized by Projekt DEAL. This project was funded by the National Cooperative for the Disposal of Radioactive Waste (Nagra) and the Leibniz Institute for Applied Geophysics (LIAG).

Availability of data and materials

The datasets presented in this study are available in Scheidt et al. (2023).

Declarations

Ethics approval and consent to participate
Not applicable.

Competing interests
Neither the author nor the co-authors have any financial or non-financial competing interests to declare.

Received: 9 February 2023 Accepted: 12 June 2023
Published online: 31 July 2023

References
Akçar, N., Ivy-Ochs, S., Alfimov, V., Claude, A., Graf, H. R., Dehnert, A., Kubik, P. W., Rahn, M., Kuhlemann, J., & Schlüchter, C. (2014). The first major incision of the Swiss Deckenschotter landscape. *Swiss Journal of Geosciences, 107*, 337–347. https://doi.org/10.1007/s00015-014-0176-6

Akçar, N., Ivy-Ochs, S., Alfimov, V., Schlunegger, F., Claude, A., Reber, R., Christl, M., Vockenhuber, C., Dehnert, A., Rahn, M., & Schlüchter, C. (2017). Isochron-burial dating of glaciofluvial deposits: First results from the Swiss Alps. *Earth Surface Processes and Landforms, 42*, 2414–2425. https://doi.org/10.1002/esp.4201

Almeida, T. P., Kasama, T., Muxworthy, A. R., Williams, W., Nagy, L., Hansen, T. W., Brown, P. D., & Dunin-Borkowski, R. E. (2014). Visualized effect of oxidation on magnetic recording fidelity in pseudo-single-domain magnetite particles. *Nature Communications, 5*, 5154. https://doi.org/10.1038/ncomms6154

Besse, J., & Courtillot, V. (2002). Apparent and true polar wander and the geometry of the geomagnetic field over the last 200 Myr. *Journal of Geophysical Research: Solid Earth, 107*, EPM6. https://doi.org/10.1029/2000JB000050

Biedermann, A. R., Jackson, M., Bilardello, D., & Feinberg, J. M. (2019). Anisotropy of (partial) isothermal remanent magnetization: DC-field-dependence and additivity. *Geophysical Journal International, 218*, 1428–1441. https://doi.org/10.1093/gji/ggz234

Bilardello, D., & Kodama, K. P. (2009). Measuring remanence anisotropy of hematite in red beds: Anisotropy of high-field isothermal remanence magnetization (hf-AIR). *Geophysical Journal International, 178*, 1260–1272. https://doi.org/10.1111/j.1365-246X.2009.04231.x

Bitterli-Dreher, P., Graf, H. R., Naef, H., Diebold, P., Matousek, F., Burger, H. & Pauli-Gabi, T. (2007). Geologischer Atlas der Schweiz. *1070 Baden (Atlasblatt 120). Erläuterungen*. Wabern: Bundesamt für Landestopografie. swisstopo.

Bolliger, T., Fejfar, O., Graf, H., & Kälin, D. (1996). Vorläufige Mitteilung über Funde von pliozänen Kleinsäugern aus den höheren Deckenschottern des Irchels (Kt. Zürich). *Eclogae Geologicae Helvetiae, 89*, 1043–1048.

Brown, L. L., & McEnroe, S. A. (2004). Palaeomagnetism of the Egersund-Ogna anorthosite, Rogaland, Norway, and the position of Fennoscandia in the Late Proterozoic. *Geophysical Journal International, 158*, 479–488. https://doi.org/10.1111/j.1365-246X.2004.02349.x

Chadima, M., & Hrouda, F. (2006). Remasoft 3.0 a user-friendly paleomagnetic data browser and analyzer. *Travaux Géophysiques, 27*, 20–21.

Channell, J. E. T., Singer, B. S., & Jicha, B. R. (2020). Timing of Quaternary geomagnetic reversals and excursions in volcanic and sedimentary archives. *Quaternary Science Reviews, 228*, 106114. https://doi.org/10.1016/j.quascirev.2019.106114

Claude, A., Akçar, N., Ivy-Ochs, S., Schlunegger, F., Kubik, P. W., Christl, M., Vockenhuber, C., Kuhlemann, J., Rahn, M., & Schlüchter, C. (2019). Changes in landscape evolution patterns in the northern Swiss Alpine Foreland during the mid-Pleistocene revolution. *GSA Bulletin, 131*, 2056–2078. https://doi.org/10.1130/b31880.1

Claude, A., Akçar, N., Ivy-Ochs, S., Schlunegger, F., Rentzel, P., Pümpin, C., Tikhomirov, D., Kubik, P. W., Vockenhuber, C., & Dehnert, A. (2017). Chronology of Quaternary terrace deposits at the locality Hohle Gasse (Pratteln, NW Switzerland). *Swiss Journal of Geosciences, 110*, 793–809. https://doi.org/10.1007/s00015-017-0278-z

Coe, R. S. (1966). Analysis of magnetic shape anisotropy using second-rank tensors. *Journal of Geophysical Research, 71*, 2637–2644.

Cuenca-Bescós, G. (2015). The Pleistocene small mammals from Irchel, Switzerland—a taxonomic & biostratigraphic revision. *Technical report, Expertenbericht*. Brugg, Schweiz: Swiss National Nuclear Safety Inspectorate (ENSI).

Cui, Y., Verosub, K. L., & Roberts, A. P. (1994). The effect of low-temperature oxidation on large multi-domain magnetite. *Geophysical Research Letters, 21*, 757–760. https://doi.org/10.1029/94GL00639

Dankers, P. (1981). Relationship between median destructive field and remanent coercive forces for dispersed natural magnetite, titanomagnetite and hematite. *Geophysical Journal International, 64*, 447–461. https://doi.org/10.1111/j.1365-246X.1981.tb02676.x

Day, R., Fuller, M., & Schmidt, V. A. (1977). Hysteresis properties of titanomagnetites; grain-size and compositional dependence. *Physics of the Earth and Planetary Interiors, 13*, 260–267. https://doi.org/10.1016/0031-9201(77)90108-X

Diebold, P., Bitterli Brunner, P. & Naef, H. (2005). Geologischer Atlas der Schweiz. *Blatt 1069/1049 Frick-Laufenburg (Atlasblatt 110)*. Wabern: Bundesamt für Landestopografie. Swisstopo.

Dieleman, C., Christl, M., Vockenhuber, C., Gautschi, P., & Akçar, N. (2022). Early Pleistocene complex cut-and-fill sequences in the Alps. *Swiss Journal of Geosciences, 115*, 1–25. https://doi.org/10.1186/s00015-022-00411-2

Doppler, G., Kroemer, E., Rögner, K., Wallner, J., Jerz, H., & Grottenthaler, W. (2011). Quaternary stratigraphy of Southern Bavaria. *E & G (quaternary Science Journal), 60*, 329–365. https://doi.org/10.3285/eg.60.2-3.08

Dunlop, D. J. (2002). Theory and application of the Day plot (Mrs/Ms versus Hcr/Hc) 1. Theoretical curves and tests using titanomagnetite data. *Journal of Geophysical Research: Solid Earth (1978–2012), 107*, EPM4. https://doi.org/10.1029/2001JB000486

Ellwanger, D., Wielandt-Schuster, U., Franz, M., & Simon, T. (2011). The quaternary of the southwest German Alpine Foreland (Bodensee-Oberschwaben, Baden-Württemberg, Southwest Germany). *E & G (quaternary Science Journal), 60*, 306–328. https://doi.org/10.3285/eg.60.2-3.07

Fabian, K. (2006). Approach to saturation analysis of hysteresis measurements in rock magnetism and evidence for stress dominated magnetic anisotropy in young mid-ocean ridge basalt. *Physics of the Earth and Planetary Interiors, 154*, 299–307. https://doi.org/10.1016/j.pepi.2005.06.016

Fassbinder, J. W., & Stanjek, H. (1994). Magnetic properties of biogenic soil greigite (Fe_3S_4). *Geophysical Research Letters, 21*, 2349–2352. https://doi.org/10.1029/94GL02506

Fejfar, O., Heinrich, W.D. (1990). Muroid rodent biochronology of the Neogene and Quaternary in Europe. In: *European Neogene mammal chronology*. Plenum Press, New York.

Fischer, G. & Schnegg, P.-A. (1979b). Inklinationskarte der Schweiz 1:500 000. Wabern: Bundesamt für Landestopografie swisstopo

Fischer, G. & Schnegg, P.-A. (1979a). Deklinationskarte der Schweiz 1:500 000. Wabern: Bundesamt für Landestopografie swisstopo

Fisher, R. (1953). Dispersion on a sphere. *Proceedings of the Royal Society of London, 217A*, 295–305.

Fleming, E. J., Lovell, H., Stevenson, C. T. E., Petronis, M. S., Benn, D. I., Hambrey, M. J., & Fairchild, I. J. (2013). Magnetic fabrics in the basal ice of a surge-type glacier. *Journal of Geophysical Research: Earth Surface, 118*, 2263–2278. https://doi.org/10.1002/jgrf.20144

France, D., & Oldfield, F. (2000). Identifying goethite and hematite from rock magnetic measurements of soils and sediments. *Journal of Geophysical Research: Solid Earth, 105*, 2781–2795. https://doi.org/10.1029/1999JB900304

Frei, R. (1912). Monographie des schweizerischen Deckenschotters. *Beiträge zur geologischen Karte der Schweiz 37 (N.F.)*. A. Francke.

Ge, K., & Williams, W. (2020). Effects of transition zone on magnetic properties of low temperature oxidation of magnetite particle:comparison of experiment and micromagnetic modeling. *IOP Conference Series Materials Science and Engineering, 840*, 012007. https://doi.org/10.1088/1757-899x/840/1/012007

Gehring, A. U., Fischer, H., Louvel, M., Kunze, K., & Weidler, P. G. (2009). High temperature stability of natural maghemite: A magnetic and spectroscopic study. *Geophysical Journal International, 179*, 1361–1371. https://doi.org/10.1111/j.1365-246X.2009.04348.x

Gendler, T. S., Shcherbakov, V. P., Dekkers, M. J., Gapeev, A. K., Gribov, S. K., & McClelland, E. (2005). The lepidocrocite-maghemite-haematite reaction chain-I. Acquisition of chemical remanent magnetization by maghemite, its magnetic properties and thermal stability. *Geophysical Journal International, 160*, 815–832. https://doi.org/10.1111/j.1365-246X.2005.02550.x

Graf, H. R. (1993). *Die Deckenschotter der zentralen Nordschweiz*. PhD, ETH Zurich.

Graf, H. R. (1996). Caliche-Bildungen auf Höheren Deckenschottern der Nordschweiz? *E&G Quaternary Science Journal, 46*, 48–53. https://doi.org/10.3285/eg.46.1.04

Graf, H. R. (2009). Stratigraphie und Morphogenese von frühpleistozänen Ablagerungen zwischen Bodensee und Klettgau. *E&G Quaternary Science Journal, 58*, 12–54. https://doi.org/10.3285/eg.58.1.02

Graf, H. R. (2019). Die Höheren Deckenschotter von Albis, Uetliberg und Heitersberg. *Swiss Bulletin Der Angewandten Geologie, 24*, 3–25.

Graf, H. R., & Burkhalter, R. (2016). Quaternary deposits: Concept for a stratigraphic classification and nomenclature—an example from northern Switzerland. *Swiss Journal of Geosciences, 109*, 137–147. https://doi.org/10.1007/s00015-016-0222-7

Griffiths, D., King, R., Rees, A., & Wright, A. E. (1960). The remanent magnetism of some recent varved sediments. *Proceedings of the Royal Society of London. Series a. Mathematical and Physical Sciences, 256*, 359–383. https://doi.org/10.1098/rspa.1960.0113

Gubler, T. (1996). *Der Üetliberg—Ein Archiv von 320 Mio. Jahren Erdgeschichte,* Stäubli AG, Zürich, Stiftung für die Erforschung des Üetlibergs.

Gubler, T. (2009). Geologischer Atlas der Schweiz. *Blatt 1111 Albis (Atlasblatt 134). Erläuterungen*. Wabern: Bundesamt für Landestopografie. swisstopo.

Güller, A. (1944). Über den Deckenschotter am Südhang der Lägern (Kt. Zürich). *Eclogae Geologicae Helvetiae, 37*, 189–193.

Haeuselmann, P., Granger, D. E., Jeannin, P.-Y., & Lauritzen, S.-E. (2007). Abrupt glacial valley incision at 0.8 Ma dated from cave deposits in Switzerland. *Geology, 35*, 143–146.

Haldimann, P., Graf, H. R. & Jost, J. (2017). Geologischer Atlas der Schweiz. *Blatt 1071 Bülach (Atlasblatt 151), Erläuterungen*. Wabern: Bundesamt für Landestopografie. swisstopo.

Hantke, R. (1962). Zur Altersfrage des höheren und des tieferen Deckenschotters in der Nordostschweiz. *Vierteljahrsschrift der Naturforschenden Gesellschaft in Zürich, 11*.

Harrison, R. J., & Putnis, A. (1996). Magnetic properties of the magnetite-spinel solid solution: Curie temperatures, magnetic susceptibilities, and cation ordering. *American Mineralogist, 81*, 375–384. https://doi.org/10.2138/am-1996-3-412

Heider, F., & Dunlop, D. J. (1987). Two types of chemical remanent magnetization during the oxidation of magnetite. *Physics of the Earth and Planetary Interiors, 46*, 24–45. https://doi.org/10.1016/0031-9201(87)90169-5

Heider, F., Dunlop, D. J., & Soffel, H. C. (1992). Low-temperature and alternating field demagnetization of saturation remanence and thermoremanence in magnetite grains (0.037 μm to 5 mm). *Journal of Geophysical Research: Solid Earth, 97*, 9371–9381. https://doi.org/10.1029/91JB03097

Hofmann, F. & Hantke, R. (1964). Geologischer Atlas der Schweiz. . *Blatt 1032 Diessenhofen mit Anhängsel von Blatt 1031 Neunkirch (Atlasblatt 38), Erläuterungen*. Wabern: Bundesamt für Landestopografie, swisstopo.

Hrouda, F. (1982). Magnetic anisotropy of rocks and its application in geology and geophysics. *Geophysical Surveys, 5*, 37–82. https://doi.org/10.1007/BF01450244

Jelínek, V. (1977). The statistical theory of measuring anisotropy of magnetic susceptibility of rocks and its application. Geofyzika, Brno: Czech Republic.

Jelinek, V. (1981). Characterization of the magnetic fabric of rocks. *Tectonophysics, 79*, T63–T67. https://doi.org/10.1016/0040-1951(81)90110-4

Jelinek, V. (1996). Measuring anisotropy of magnetic susceptibility on a slowly spinning specimen—basic theory (AGICO print No. 10).

Jiang, Z., Liu, Q., Dekkers, M. J., Tauxe, L., Qin, H., Barrón, V., & Torrent, J. (2015). Acquisition of chemical remanent magnetization during experimental ferrihydrite–hematite conversion in Earth-like magnetic field—implications for paleomagnetic studies of red beds. *Earth and Planetary Science Letters, 428*, 1–10. https://doi.org/10.1016/j.epsl.2015.07.024

Jiang, Z., Liu, Q., Roberts, A. P., Barrón, V., Torrent, J., & Zhang, Q. (2018). A new model for transformation of ferrihydrite to hematite in soils and sediments. *Geology, 46*, 987–990. https://doi.org/10.1130/G45386.1

Jiang, Z., Liu, Q., Roberts, A. P., Dekkers, M. J., Barrón, V., Torrent, J., & Li, S. (2022). The magnetic and color reflectance properties of hematite: From Earth to Mars. *Reviews of Geophysics, 60*, e2020RG000698. https://doi.org/10.1029/2020RG000698

Jiang, Z., Liu, Q., Zhao, X., Roberts, A. P., Heslop, D., Barrón, V., & Torrent, J. (2016). Magnetism of Al-substituted magnetite reduced from Al-hematite. *Journal of Geophysical Research: Solid Earth, 121*, 4195–4210. https://doi.org/10.1002/2016JB012863

Johnson, H., Lowrie, W., & Kent, D. V. (1975). Stability of anhysteretic remanent magnetization in fine and coarse magnetite and maghemite particles. *Geophysical Journal International, 41*, 1–10. https://doi.org/10.1111/j.1365-246X.1975.tb05480.x

Johnson, H., & Merrill, R. (1973). Low-temperature oxidation of a titanomagnetite and the implications for paleomagnetism. *Journal of Geophysical Research, 78*, 4938–4949. https://doi.org/10.1029/JB078i023p04938

Knudsen, M. F., Nørgaard, J., Grischott, R., Kober, F., Egholm, D. L., Hansen, T. M., & Jansen, J. D. (2020). New cosmogenic nuclide burial-dating model indicates onset of major glaciations in the Alps during Middle Pleistocene Transition. *Earth and Planetary Science Letters, 549*, 116491. https://doi.org/10.1016/j.epsl.2020.116491

Kuhlemann, J. & Rahn, M. (2013). Plio-Pleistocene landscape evolution in Northern Switzerland. *Swiss Journal of Geosciences 106*, 451–467. https://doi.org/10.1007/s00015-013-0152-6

Lisiecki, L. E., & Raymo, M. E. (2005). A Pliocene-Pleistocene stack of 57 globally distributed benthic δ^{18}O records. *Paleoceanography, 20*, 1–17. https://doi.org/10.1029/2004PA001071

Maher, B. A. (1986). Characterisation of soils by mineral magnetic measurements. *Physics of the Earth and Planetary Interiors, 42*, 76–92. https://doi.org/10.1016/S0031-9201(86)80010-3

Maher, B. A., Alekseev, A., & Alekseeva, T. (2003). Magnetic mineralogy of soils across the Russian Steppe: Climatic dependence of pedogenic magnetite formation. *Palaeogeography, Palaeoclimatology, Palaeoecology, 201*, 321–341. https://doi.org/10.1016/S0031-0182(03)00618-7

Maher, B. A., & Taylor, R. M. (1988). Formation of ultrafine-grained magnetite in soils. *Nature, 336*, 368–370. https://doi.org/10.1038/336368a0

Matousek, F., Wanner, M., Baumann, A., Graf, H. R., Nüesch, R. & Bitterli, T. (2000). Geologischer Atlas der Schweiz. *Blatt 1050 Zurzach (Atlasblatt 102), Karte* Wabern: Bundesamt für Landestopografie. swisstopo.

McCabe, C., Jackson, M., & Ellwood, B. B. (1985). Magnetic anisotropy in the Trenton limestone: Results of a new technique, anisotropy of anhysteretic susceptibility. *Geophysical Research Letters, 12*, 333–336. https://doi.org/10.1029/GL012i006p00333

Nishitani, T., & Kono, M. (1983). Curie temperature and lattice constant of oxidized titanomagnetite. *Geophysical Journal International, 74*, 585–600. https://doi.org/10.1111/j.1365-246X.1983.tb01890.x

NOAA. 2022. *Magnetic Field Calculators* [Online]. U.S. Department of Commerce. Available: https://www.ngdc.noaa.gov/geomag/calculators/magcalc.shtml. Accessed 04 May 2022.

Özdemir, Ö. & Dunlop, D. J. (2005). Thermoremanent magnetization of multidomain hematite. *Journal of Geophysical Research: Solid Earth, 110*. https://doi.org/10.1029/2005JB003820

Özdemir, Ö., & Dunlop, D. J. (1996). Thermoremanence and Néel temperature of goethite. *Geophysical Research Letters, 23*, 921–924. https://doi.org/10.1029/96GL00904

Pavoni, N., Schindler, C., Freimoser, M. & Haldimann, P. (1992). Geologischer Atlas der Schweiz *Blatt 1091 Zürich (Atlasblatt 90), Karte*. Wabern: Bundesamt für Landestopografie. swisstopo.

Penck, A. & Brückner, E. (1909). *Die alpen im Eiszeitalter*, Tauchnitz.

Preusser, F., Graf, H. R., Keller, O., Krayss, E., & Schlüchter, C. (2011). Quaternary glaciation history of northern Switzerland. *E&G Quaternary Science Journal, 60*, 21. https://doi.org/10.3285/eg.60.2-3.06

Raffi, I., Wade, B., Pälike, H., Beu, A., Cooper, R., Crundwell, M., Krijgsman, W., Moore, T., Raine, I., Sardella, R. (2020). The neogene period. In: *Geologic time scale*. Elsevier.

Rezanezhad, F., Couture, R., Kovac, R., O'Connell, D., & van Cappellen, P. (2014). Water table fluctuations and soil biogeochemistry: An experimental approach using an automated soil column system. *Journal of Hydrology, 509*, 245–256. https://doi.org/10.1016/j.jhydrol.2013.11.036

Roberts, A. P., Cui, Y., & Verosub, K. L. (1995). Wasp-waisted hysteresis loops: Mineral magnetic characteristics and discrimination of components in mixed magnetic systems. *Journal of Geophysical Research: Solid Earth, 100*, 17909–17924. https://doi.org/10.1029/95jb00672

Roberts, A. P., Hu, P., Harrison, R. J., Heslop, D., Muxworthy, A. R., Oda, H., Sato, T., Tauxe, L., & Zhao, X. (2019). Domain state diagnosis in rock magnetism: evaluation of potential alternatives to the Day diagram. *Journal of Geophysical Research Solid Earth*. https://doi.org/10.1029/2018JB017049

Rolf, C., Fromm, K. & Ellwanger, D. (2012). Zur Magnetostratigraphie an Deckenschottern aus dem südlichen Oberschwaben. *Zur Magnetostratigraphie an Deckenschottern aus dem südlichen Oberschwaben.* Freiburg i.Br.: Rgierungspräsidium Freiburg, Landesamt für Geologie, Rohstoffe und Bergbau.

Rowan, C. J., & Roberts, A. P. (2006). Magnetite dissolution, diachronous greigite formation, and secondary magnetizations from pyrite oxidation: Unravelling complex magnetizations in Neogene marine sediments from New Zealand. *Earth and Planetary Science Letters, 241*, 119–137. https://doi.org/10.1016/j.epsl.2005.10.017

Scheidt, S., Egli, R., & Biedermann, A. R. (2023). Palaeomagnetic and mineral magnetic investigations on fine-grained deposits of the Deckenschotter in Switzerland and Germany. figshare: figshare. https://doi.org/10.6084/m9.figshare.c.6414254

Schlunegger, F., & Hinderer, M. (2001). Crustal uplift in the Alps: Why the drainage pattern matters. *Terra Nova, 13*, 425–432. https://doi.org/10.1046/j.1365-3121.2001.00374.x

Schwertmann, U. (1988). *Occurrence and formation of iron oxides in various pedoenvironments*. Springer: Iron in soils and clay minerals.

Snowball, I. (1997). Gyroremanent magnetization and the magnetic properties of greigite-bearing clays in southern Sweden. *Geophysical Journal International, 129*, 624–636. https://doi.org/10.1111/j.1365-246X.1997.tb04498.x

Stephenson, A., & Snowball, I. F. (2001). A large gyromagnetic effect in greigite. *Geophysical Journal International, 145*, 570–575. https://doi.org/10.1046/j.0956-540x.2001.01434.x

Swanson-Hysell, N. L., Fairchild, L. M., & Slotznick, S. P. (2019). Primary and secondary red bed magnetization constrained by fluvial intraclasts. *Journal of Geophysical Research: Solid Earth, 124*, 4276–4289. https://doi.org/10.1029/2018JB017067

Tan, X., Kodama, K. P., & Fang, D. (2002). Laboratory depositional and compaction-caused inclination errors carried by haematite and their implications in identifying inclination error of natural remanence in red beds. *Geophysical Journal International, 151*, 475–486. https://doi.org/10.1046/j.1365-246X.2002.01794.x

Tanty, C., Valet, J.-P., Carlut, J., Bassinot, F., & Zaragosi, S. (2016). Acquisition of detrital magnetization in four turbidites. *Geochemistry, Geophysics, Geosystems, 17*, 3207–3223. https://doi.org/10.1002/2016GC006378

Tauxe, L., & Kent, D. V. (1984). Properties of a detrital remanence carried by haematite from study of modern river deposits and laboratory redeposition experiments. *Geophysical Journal International, 76*, 543–561. https://doi.org/10.1111/j.1365-246X.1984.tb01909.x

Tauxe, L., Mullender, T., & Pick, T. (1996). Potbellies, wasp-waists, and superparamagnetism in magnetic hysteresis. *Journal of Geophysical Research, 101*, 571–583. https://doi.org/10.1029/95JB03041

Taylor, R., Maher, B., & Self, P. (1986). Magnetite in soils: I. The synthesis of single-domain and superparamagnetic magnetite. *Clay Minerals, 22*, 411–422. https://doi.org/10.1180/claymin.1987.022.4.05

Valla, P. G., Shuster, D. L., & van der Beek, P. A. (2011). Significant increase in relief of the European Alps during mid-Pleistocene glaciations. *Nature Geoscience, 4*, 688–692. https://doi.org/10.1038/ngeo1242

Weber, A. (1930). Die glazialgeologie des Tösstales und ihre Beziehungen zur Diluvialgeschichte der Nordostschweiz. *Mitteilungen der Naturwissenschaftlichen Gesellschaft in Winterthur,* 17–18.

www.Strati.ch 2022. Lithostratigraphisches Lexikon der Schweiz. *Quartär.* www.strati.ch: Swisstopo, Bundesamt für Landestopografie - Akademie der Naturwissenschaften Schweiz.

Zaugg, A., Geyer, M., Rahn, M., Wessels, M., Schlichtherle, H., Hasenfratz, A. & Burkhalter, R. (2008). Steckborn-Kreuzlingen (CN 1033/1034). *Karte mit Erläuterungen zum Geologischen Atlas der Schweiz 1:25 000.* Wabern: Bundesamt für Landestopografie swisstopo.

Zollinger, G. (1991). Zur Landschaftsgenese und Quartärstratigraphie am Südlichen Oberrheingraben-am Beispiel der Lössdeckschichten der ziegelei in Allschwil (Kanton Basel-Landschaft). *Eclogae Geologicae Helvetiae, 84*, 739–752.

Publisher's Note